Dark radiation and inflationary freedom after Planck 2015

Eleonora Di Valentino, Stefano Gariazzo, Martina Gerbino, Elena Giusarma, Olga Mena

PHYSICAL REVIEW D **93,** 083523 (2016)

Dark radiation and inflationary freedom after Planck 2015

Eleonora Di Valentino,[1,*] Stefano Gariazzo,[2,3] Martina Gerbino,[4,5,6] Elena Giusarma,[6,7] and Olga Mena[8]

[1]*Institut d'Astrophysique de Paris, UMR7095: CNRS & UPMC- Sorbonne Universities, F-75014 Paris, France*

[2]*Department of Physics, University of Torino, Via P. Giuria 1, I-10125 Torino, Italy*

[3]*INFN, Sezione di Torino, Via P. Giuria 1, I-10125 Torino, Italy*

[4]*The Oskar Klein Centre for Cosmoparticle Physics, Department of Physics, Stockholm University, AlbaNova, SE-106 91 Stockholm, Sweden*

[5]*Nordita Nordic Institute for Theoretical Physics, Roslagstullsbacken 23, SE-106 91 Stockholm, Sweden*

[6]*Physics Department and INFN, Università di Roma "La Sapienza", P.le Aldo Moro 2, 00185 Rome, Italy*

[7]*McWilliams Center for Cosmology, Department of Physics, Carnegie Mellon University, Pittsburgh, Pennsylvania 15213, USA*

[8]*IFIC, Universidad de Valencia-CSIC, 46071 Valencia, Spain*

(Received 3 February 2016; published 28 April 2016)

The simplest inflationary models predict a primordial power spectrum (PPS) of the curvature fluctuations that can be described by a power-law function that is nearly scale invariant. It has been shown, however, that the low-multipole spectrum of the cosmic microwave background anisotropies may hint at the presence of some features in the shape of the scalar PPS, which could deviate from its canonical power-law form. We study the possible degeneracies of this nonstandard PPS with the active neutrino masses, the effective number of relativistic species, and a sterile neutrino or a thermal axion mass. The limits on these additional parameters are less constraining in a model with a nonstandard PPS when including only the temperature autocorrelation spectrum measurements in the data analyses. The inclusion of the polarization spectra noticeably helps in reducing the degeneracies, leading to results that typically show no deviation from the ΛCDM model with a standard power-law PPS. These findings are robust against changes in the function describing the noncanonical PPS. Albeit current cosmological measurements seem to prefer the simple power-law PPS description, the statistical significance to rule out other possible parametrizations is still very poor. Future cosmological measurements are crucial to improve the present PPS uncertainties.

DOI: 10.1103/PhysRevD.93.083523

I. INTRODUCTION

Inflation is one of the most successful theories that explains the so-called *horizon* and *flatness* problems, providing an origin for the primordial density perturbations that evolved to form the structures we observe today [1–11]. The standard inflationary paradigm predicts a simple shape for the primordial power spectrum (PPS) of scalar perturbations; in this context, the PPS can be described by a power-law expression. However, there also exist more complicated inflationary scenarios which can give rise to nonstandard PPS forms, with possible features at different scales; see, e.g., Refs. [12,13] and the reviews [14,15].

The usual procedure to reconstruct the underlying PPS is to assume a model for the evolution of the Universe and calculate the transfer function and then use different techniques to constrain a completely unknown PPS, comparing the theoretical prediction with the measured power spectrum of the cosmic microwave background radiation (CMB). Among the methods developed in the past, we can list regularization methods such as the Richardson-Lucy iteration [16–19], truncated singular value decomposition [20], and Tikhonov regularization [21,22] or methods such as the maximum entropy deconvolution [23] or the *cosmic inversion* methods [24–28]. Recently, the Planck Collaboration presented a wide discussion about constraints on inflation [29]. All these methods provide a hint for a PPS which may not be as simple as a power law. While the significance of the deviations is small for some cases, it is interesting to note that the CMB temperature power spectra as measured by both WMAP [30] and Planck [31,32] show similar results: the differences from the power law are located in the low-multipole region. These deviations could arise from some statistical fluctuations or, instead, result from a nonstandard inflationary mechanism.

If the features we observe are the result of a nonstandard inflationary mechanism, we may be using an incomplete parametrization for the PPS in our cosmological analyses. It has been shown that this could lead to biased results in the cosmological constraints of different quantities. Namely, the constraints on the dark radiation properties [33–35] or on non-Gaussianities [36] can be distorted, leading to spurious conclusions. In this work, we aim to study the impact of a general PPS form in the constraints obtained for

*valentin@iap.fr

the properties of dark radiation candidates, such as the active neutrino masses and their effective number, sterile neutrino species, and thermal axion properties. The outline of the paper is as follows. We present the baseline standard ΛCDM cosmological model, the PPS parametrization, and the cosmological data in Sec. II. The results obtained within the ΛCDM framework are presented in Sec. III. Concerning possible extensions of the ΛCDM scenario, we study the constraints on the effective number of relativistic species in Sec. IV, on the neutrino masses in Sec. V, on massive neutrinos with a varying effective number of relativistic species in Sec. VI, on massive sterile neutrinos in Sec. VII, and on the thermal axion properties in Sec. VIII. Finally, in Sec. IX, we show the reconstructed PPS shape, comparing different possible approaches, and we draw our conclusions in Sec. X.

II. BASELINE MODEL AND COSMOLOGICAL DATA

In this section, we outline the baseline theoretical model that will be extended to study the dark radiation properties. For our analyses, we use the numerical Boltzmann solver `CAMB` [37] for the theoretical spectra calculation and the Markov chain Monte Carlo (MCMC) algorithm `CosmoMC` [38] to sample the parameter space.

A. Standard cosmological model

The baseline model that we will extend to study various dark radiation properties is the ΛCDM model, described by the six usual parameters: the current energy density of baryons and of cold dark matter (CDM) ($\Omega_b h^2$, $\Omega_c h^2$), the ratio between the sound horizon and the angular diameter distance at decoupling (θ), the optical depth to reionization (τ), plus two parameters that describe the PPS of scalar perturbations, $P_s(k)$. The simplest models of inflation predict a power-law form for the PPS,

$$P_s(k) = A_s(k/k_*)^{n_s-1}, \tag{1}$$

where $k_* = 0.05$ Mpc^{-1} is the pivot scale, while the amplitude (A_s) and the scalar spectral index (n_s) are free parameters in the ΛCDM model. From these fundamental cosmological parameters, we will compute other derived quantities, such as the Hubble parameter today H_0 and the clustering parameter σ_8, defined as the mean of matter fluctuations inside a sphere of $8h$ Mpc radius.

From what concerns the remaining cosmological parameters, we follow the values of Ref. [39]. In particular, unless they are freely varying, we consider the sum of the active neutrino masses to be $\Sigma m_\nu = 0.06$ eV and the effective number of relativistic species to be $N_{\rm eff} = 3.046$ [40].

B. Primordial power spectrum of scalar perturbations

As stated before, possible hints of a nonstandard PPS of scalar perturbations were found in several analyses, including both the WMAP and the Planck CMB spectra [16–29,34,35]. From the theoretical point of view, there are plenty of well-motivated inflationary models that can give rise to nonstandard PPS forms. Our major goal here is to study the robustness of the constraints on different cosmological quantities vs a change in the assumed PPS. Several cosmological parameters are known to present degeneracies with the standard PPS parameters such as, for example, the existing one between effective number of relativistic species $N_{\rm eff}$ and the tilt of the power-law PPS n_s. These degeneracies could be even stronger when more freedom is allowed for the PPS shape. We adopt here a nonparametric description for the PPS of scalar perturbations: we describe the function $P_s(k)$ as the interpolation among a series of nodes at fixed wave modes k. Unless otherwise stated, we shall consider 12 nodes k_j ($j \in [1, 12]$) that cover a wide range of values of k; the most interesting range is explored between $k_2 = 0.001$ Mpc^{-1} and $k_{11} = 0.35$ Mpc^{-1}, which is approximately the range of wave modes probed by CMB experiments. In this range, we use equally spaced nodes in $\log k$. Additionally, we consider $k_1 = 5 \times 10^{-6}$ Mpc^{-1} and $k_{12} = 10$ Mpc^{-1} in order to ensure that all the PPS evaluations are inside the covered range. We expect that the nodes at these extreme wave modes are unconstrained by the data.

Having fixed the position of all the nodes, the free parameters that are involved in our MCMC analyses are the values of the PPS at each node, $P_{s,j} = P_s(k_j)/P_0$, where P_0 is the overall normalization, $P_0 = 2.2 \times 10^{-9}$ [39]. We use a flat prior in the interval [0.01, 10] for each $P_{s,j}$, for which the expected value will be close to 1.

The complete $P_s(k)$ is then described as the interpolation among the points $P_{s,j}$,

$$P_s(k) = P_0 \times \texttt{PCHIP}(k; P_{s,1}, \ldots, P_{s,12}), \tag{2}$$

where `PCHIP` is the *piecewise cubic Hermite interpolating polynomial* [41,42] (see also Ref. [34] for a detailed description[1]). In the following, when presenting our results, we will compare the constraints obtained in the context of the standard ΛCDM model with a standard power-law PPS to those obtained with the free `PCHIP` PPS, described by (at least) 16 free parameters ($\Omega_b h^2$, $\Omega_c h^2$, θ, τ, $P_{s,1}, \ldots, P_{s,12}$). This minimal model will be extended to include the dark radiation properties we shall study in the various analyses.

The impact of the assumptions on the PPS parametrization will also be tested. We shall compare the results obtained with 12 nodes to the ones derived using a `PCHIP` PPS described by eight nodes. The positions of these eight

[1]The `PCHIP` method is similar to the natural cubic spline, but it has the advantage of avoiding the introduction of spurious oscillations in the interpolation; this is obtained with a condition on the first derivative in the nodes, which is null if there is a change in the monotonicity of the point series.

nodes $k_j^{(8)}$ is selected with the same rules as above: equally spaced nodes in $\log k$ between $k_2^{(8)} = k_2 = 0.001$ Mpc^{-1} and $k_7^{(8)} = k_{11} = 0.35$ Mpc^{-1}, plus the external nodes $k_1^{(8)} = k_1 = 5 \times 10^{-6}$ Mpc^{-1} and $k_8^{(8)} = k_{12} = 10$ Mpc^{-1}.

To ease comparison between the power-law and the PCHIP PPS approaches, we list in all the tables the results obtained for these two schemes. When considering a power-law PPS model, we show the constraints on n_s and A_s, together with the values of the nodes $P_{s,1}^{\rm bf}$ to $P_{s,12}^{\rm bf}$ that would correspond to the best-fit values of n_s and A_s ($n_s^{\rm bf}$ and $A_s^{\rm bf}$). In other words, in each table presenting the marginalized constraints for the different cosmological parameters, in the columns corresponding to the analysis involving a power-law PPS, we shall list the values

$$P_{s,j}^{\rm bf} \equiv \frac{A_s^{\rm bf}}{P_0}\left(\frac{k_j}{k_*}\right)^{n_s^{\rm bf}-1} \quad \text{with} \quad j \in [1,\ldots,12], \tag{3}$$

which can be exploited for comparison purposes among the two PPS approaches.

C. Cosmological data

We base our analyses on the recent release from the Planck Collaboration [32], which obtained the most precise CMB determinations in a very wide range of multipoles. We consider the full temperature power spectrum at multipoles $2 \leq \ell \leq 2500$ ("Planck TT" hereafter) and the polarization power spectra in the range $2 \leq \ell \leq 29$ ("lowP"). We shall also include the cross-correlation between temperature and E-mode polarization (TE), and the E-mode polarization auto-correlation (EE) data at $30 \leq \ell \leq 2500$ ("TE, EE") [43]. Since the polarization spectra at high multipoles are still under discussion and some residual systematics were detected by the Planck Collaboration [39,43], we shall use as a baseline data set the combination "Planck TT + lowP." The impact of polarization measurements will be separately studied in the data set "Planck TT, TE, EE + lowP."

Additionally, we will consider the two CMB data sets above in combination with the following cosmological measurements:

(i) baryon acoustic oscillations (BAO) data as obtained by 6dFGS [44] at redshift $z = 0.1$, by the SDSS Main Galaxy Sample (MGS) [45] at redshift $z_{\rm eff} = 0.15$, and by the BOSS experiment in the DR11 release, both from the LOWZ and CMASS samples [46] at redshift $z_{\rm eff} = 0.32$ and $z_{\rm eff} = 0.57$, respectively;

(ii) the matter power spectrum (MPkW) as measured by the WiggleZ Dark Energy Survey [47], from measurements at four different redshifts ($z = 0.22$, $z = 0.41$, $z = 0.60$, and $z = 0.78$) for the scales $0.02h$ Mpc$^{-1} < k < 0.2h$ Mpc^{-1};

(iii) the reconstruction of the lensing potential obtained by the Planck Collaboration with the CMB trispectrum analysis [48].

III. ΛCDM MODEL

In this section, we shall consider a limited number of data combinations, including exclusively the data sets that can improve the constraints on the PCHIP PPS at small scales, namely, the Planck polarization measurements at high ℓ and the MPkW constraints on the matter power spectrum.

The results we obtain for the ΛCDM model are reported in Table I in the Appendix. In general, in the absence of high-multipole polarization or large-scale structure data, the parameter errors are increased. Those associated to $\Omega_b h^2$, $\Omega_c h^2$, H_0, and σ_8 show a larger difference, with deviations of the order of 1σ in the PCHIP PPS case with respect to the power-law PPS case. The differences between the PCHIP and the power-law PPS parametrizations are much smaller for the "Planck TT, TE, EE + lowP + MPkW" data set, and the two descriptions of the PPS give bounds for the ΛCDM parameters that fully agree. Therefore, the addition of the high-multipole polarization spectra has a profound impact in our analyses, as we carefully explain in what follows. Figure 1 depicts the CMB spectra measured by Planck [32], together with the theoretical spectra obtained from the best-fit values arising from our analyses. More concretely, we use the marginalized best-fit values reported in Table I for the ΛCDM model with a power-law PPS obtained from the analyses of the Planck TT + lowP (in black) and Planck TT, TE, EE + lowP (in blue) data sets, plus the best-fit values in the ΛCDM model with a PCHIP PPS, from the Planck TT + lowP (red) and Planck TT, TE, EE + lowP (green) data sets. We plot the $D_\ell = \ell(\ell+1)C_\ell/(2\pi)$ spectra of the TT, TE, and EE anisotropies, as well as the relative (absolute for the TE spectra) difference between each spectrum and the one obtained from the Planck TT + lowP data in the ΛCDM model with the power-law PPS. Notice that, in the case of the TT and EE spectra, the best-fit spectra are in good agreement with the observational data, even if there are variations among the ΛCDM parameters, as they can be compensated by the freedom in the PPS. However, in the TE cross-correlation spectrum case, such a compensation is no longer possible; the inclusion of the TE spectrum in the analyses is therefore expected to have a strong impact on the derived bounds.

IV. EFFECTIVE NUMBER OF RELATIVISTIC SPECIES

The amount of energy density of relativistic species in the Universe is usually defined as the sum of the photon contribution ρ_γ plus the contribution of all the other relativistic species. This is described by the effective number of relativistic degrees of freedom $N_{\rm eff}$,

$$\rho_{\rm rad} = \left[1 + \frac{7}{8}\left(\frac{4}{11}\right)^{4/3} N_{\rm eff}\right]\rho_\gamma, \tag{4}$$

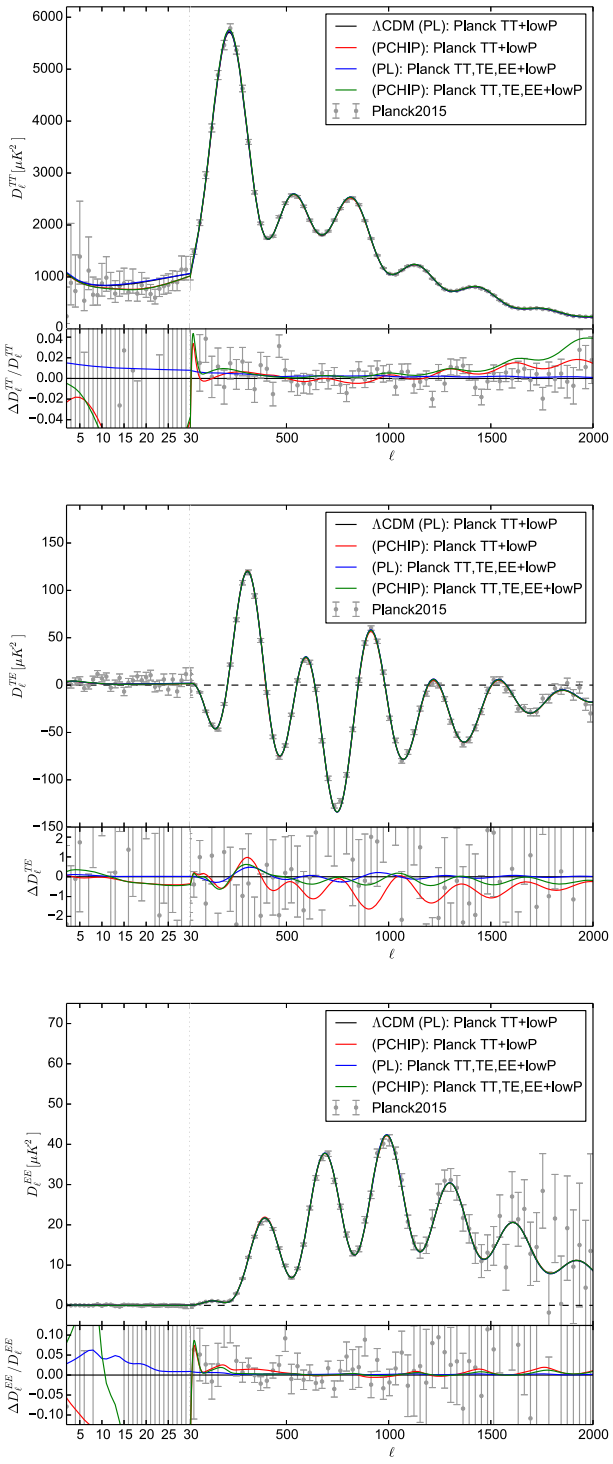

FIG. 1. Comparison of the Planck 2015 data [32] with the TT, TE, and EE spectra obtained using the marginalized best-fit values from the analyses of Planck TT + lowP (black) and Planck TT, TE, EE + lowP (blue) in the ΛCDM model with the power-law (PL) PPS and from the analyses of Planck TT + lowP (red) and Planck TT, TE, EE + lowP (green) in the ΛCDM model with the PCHIP PPS. The adopted values for each spectrum are reported in Table I. We plot the $D_\ell = \ell(\ell+1)C_\ell/(2\pi)$ spectra and the relative (absolute for the case of the TE spectra) difference between each spectrum and the one obtained in the ΛCDM (power-law PPS) model from the Planck TT + lowP data (black line).

where $N_{\rm eff} = 3.046$ [40] for the three active neutrino standard scenario. Deviations of $N_{\rm eff}$ from its standard value may indicate that the thermal history of the active neutrinos is different from what we expect or that additional relativistic particles are present in the Universe, as additional sterile neutrinos or thermal axions.

A nonstandard value of $N_{\rm eff}$ may affect the big bang nucleosynthesis era and also the matter-radiation equality. A shift in the matter-radiation equality would cause a change in the expansion rate at decoupling, affecting the sound horizon and the angular scale of the peaks of the CMB spectrum, as well as in the contribution of the *early integrated Sachs Wolfe (ISW) effect* to the CMB spectrum. To avoid such a shift and its consequences, it is possible to change simultaneously the energy densities of matter and dark energy, in order to keep fixed all the relevant scales in the Universe. In this case, the CMB spectrum will only be altered by an increased Silk damping at small scales (see, e.g., Refs. [49–52]).

The constraints on $N_{\rm eff}$ are summarized in Fig. 2, where we plot the 68% and 95% C.L. constraints on $N_{\rm eff}$ obtained with different data sets and PPS combinations for the $\Lambda{\rm CDM} + N_{\rm eff}$ model.

The introduction of $N_{\rm eff}$ as a free parameter does not change significantly the results for the ΛCDM parameters if a power-law PPS is considered. However, once the freedom in the PPS is introduced, some degeneracies between the PCHIP nodes $P_{s,j}$ and $N_{\rm eff}$ appear. Nevertheless, even if

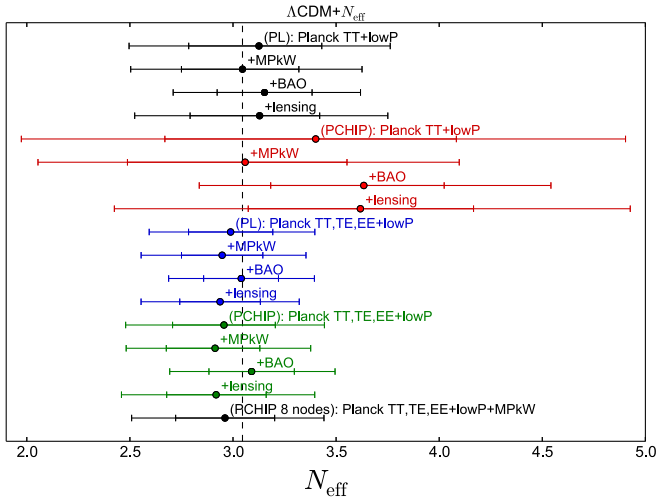

FIG. 2. 68% and 95% C.L. constraints on $N_{\rm eff}$, obtained in the $\Lambda{\rm CDM} + N_{\rm eff}$ model. Different colors indicate Planck TT + lowP with PL PPS (black), Planck TT + lowP with PCHIP PPS (red), Planck TT, TE, EE + lowP with PL PPS (blue), and Planck TT, TE, EE + lowP with PCHIP PPS (green). For each color, we plot four different data sets: from top to bottom, we have CMB only, CMB + MPkW, CMB + BAO, and CMB + lensing. We also illustrate the results, in the context of the eight-nodes parametrization, for the Planck TT, TE, EE + lowP + MPkW data set (last point in black).

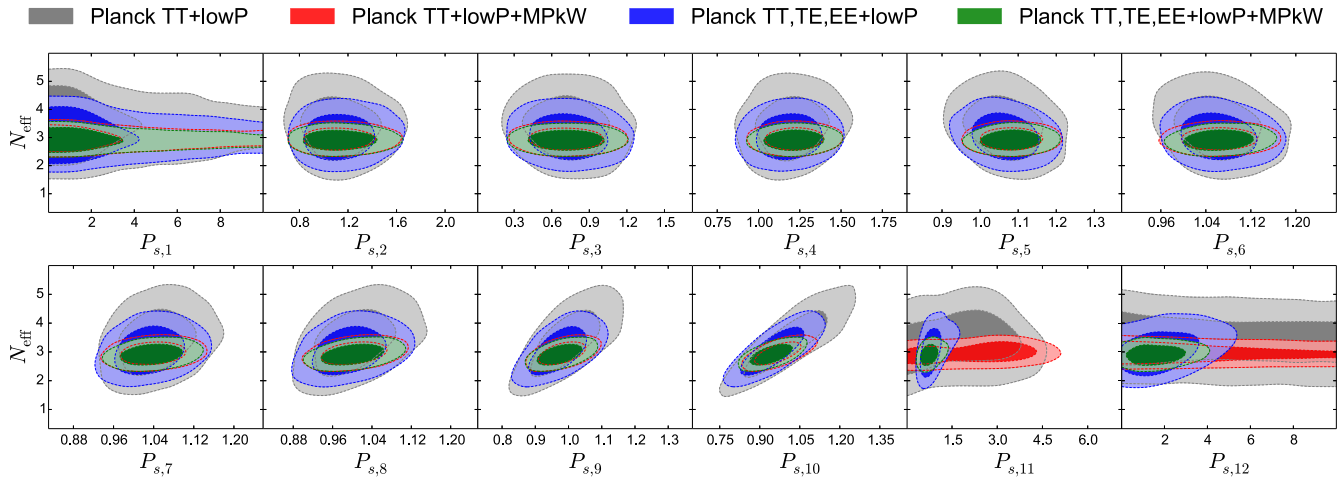

FIG. 3. 68% and 95% C.L. constraints in the ($N_{\rm eff}$, $P_{s,j}$) planes, obtained in the ΛCDM + $N_{\rm eff}$ model. We show the results for Planck TT + lowP (gray), Planck TT + lowP + MPkW (red), Planck TT, TE, EE + lowP (blue), and Planck TT, TE, EE + lowP + MPkW (green).

the constraints on $N_{\rm eff}$ are loosened for the PCHIP PPS case, all the data set combinations give constraints on $N_{\rm eff}$ that are compatible with the standard value 3.046 at 95% C.L., as we notice from Fig. 2 and Table II in the Appendix. The mild preference for $N_{\rm eff} > 3.046$ arises mainly as a volume effect in the Bayesian analysis, since the PCHIP PPS parameters can be tuned to reproduce the observed CMB temperature spectrum for a wide range of values of $N_{\rm eff}$. As expected, the degeneracy between the nodes $P_{s,j}$ and $N_{\rm eff}$ shows up at high wave modes, where the Silk damping effect is dominant; see Fig. 3. As a consequence of this correlation, the values preferred for the nodes $P_{s,6}$ to $P_{s,10}$ are slightly larger than the best-fit values in the power-law PPS at the same wave modes. The cosmological limits for a number of parameters change as a consequence of the various degeneracies with $N_{\rm eff}$. For example, to compensate the shift of the matter-radiation equality redshift due to the increased radiation energy density, the CDM energy density $\Omega_c h^2$ mean value is slightly shifted, and its constraints are weakened. At the same time, the uncertainty on the Hubble parameter H_0 is considerably relaxed, because H_0 must be also changed accordingly. The introduction of the polarization data helps in improving the constraints in the models with a PCHIP PPS, since the effects of increasing $N_{\rm eff}$ and changing the PPS are different for the temperature-temperature, the temperature-polarization, and the polarization-polarization correlation spectra, as previously discussed in the context of the ΛCDM model (see Table III in the Appendix); the preferred value of $N_{\rm eff}$ is very close to the standard value 3.046. Apparently, the Planck polarization data seem to prefer a value of $N_{\rm eff}$ slightly smaller than 3.046 for all the data sets except those including the BAO data, but the effect is not statistically significant (see the blue and green points in Fig. 2).

In conclusion, as the bounds for $N_{\rm eff}$ are compatible with 3.046, the ΛCDM + $N_{\rm eff}$ model gives results that are very close to those obtained in the simple ΛCDM model, but with slightly larger parameter uncertainties, in particular for H_0 and $\Omega_c h^2$.

V. MASSIVE NEUTRINOS

Neutrino oscillations have robustly established the existence of neutrino masses. However, neutrino mixing data only provide information on the squared mass differences and not on the absolute scale of neutrino masses. Cosmology provides an independent tool to test it, as massive neutrinos leave a non-negligible imprint in different cosmological observables [53–64]. The primary effect of neutrino masses in the CMB temperature spectrum is due to the early ISW effect. The neutrino transition from the relativistic to the nonrelativistic regime affects the decay of the gravitational potentials at the decoupling period, producing an enhancement of the small-scale perturbations, especially near the first acoustic peak. A nonzero value of the neutrino mass also induces a higher expansion rate, which suppresses the lensing potential and the clustering on scales smaller than the horizon when neutrinos become nonrelativistic. However, the largest effect of neutrino masses on the different cosmological observables comes from the suppression of galaxy clustering at small scales. After becoming nonrelativistic, the neutrino hot dark matter relics possess large velocity dispersions, suppressing the growth of matter density fluctuations at small scales. The baseline scenario we analyze here has three active massive neutrino species with degenerate masses. In addition, we consider the PPS approach outlined in Sec. II. For the numerical analyses, when considering the power-law PPS, we use the following set of parameters:

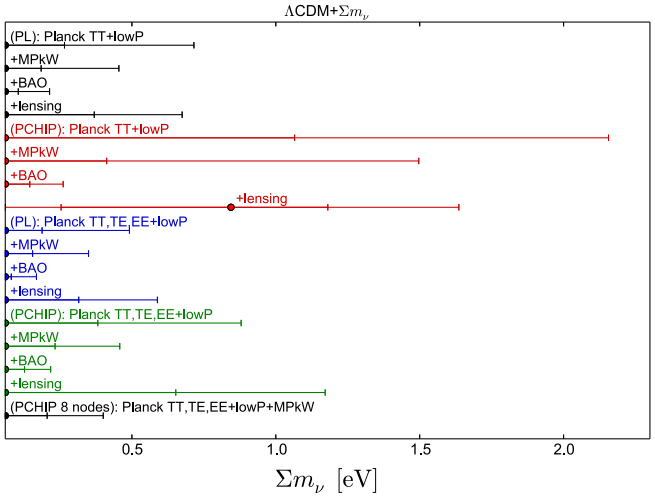

FIG. 4. As Fig. 2 but for the ΛCDM plus $\sum m_\nu$ case.

$$\{\Omega_b h^2, \Omega_c h^2, \theta, \tau, n_s, \log[10^{10} A_s], \Sigma m_\nu\}. \quad (5)$$

We then replace the n_s and A_s parameters with the other 12 extra parameters ($P_{s,i}$ with $i = 1, \ldots, 12$) related to the PCHIP PPS parametrization. The 68% and 95% C.L. bounds on Σm_ν obtained with different data set and PPS combinations are summarized in Fig. 4.

Notice that, when considering Planck TT + lowP CMB measurements plus other external data sets, for all the data combinations, the bounds on neutrino masses are weaker when considering the PCHIP PPS with respect to the power-law PPS case (see also Table IV in the Appendix). Concerning CMB data only, the bound we find in the PCHIP approach is $\Sigma m_\nu < 2.16$ eV at 95% C.L., much less constraining than the bound $\Sigma m_\nu < 0.75$ eV at 95% C.L. obtained in the power-law approach. This larger value is due to the degeneracy between Σm_ν and the nodes $P_{s,5}$ and $P_{s,6}$, as illustrated in Fig. 5. In particular, these two nodes correspond to the wave numbers where the contribution of the early ISW effect is located. Therefore, the change induced on these angular scales by a larger neutrino mass could be compensated by increasing $P_{s,5}$ and $P_{s,6}$. The addition of the matter power spectrum measurements, MPkW, leads to an upper bound on Σm_ν of 1.15 eV at 95% C.L. in the PCHIP parametrization, which is twice the value obtained when considering the power-law PPS with the same data set. The most stringent constraints on the sum of the three active neutrino masses are obtained when we use the BAO data, since the geometrical information they provide helps breaking degeneracies among cosmological parameters. In particular, we have $\Sigma m_\nu < 0.261$ eV ($\Sigma m_\nu < 0.220$ eV) at 95% C.L. when considering the PCHIP (power-law) PPS parametrization. Finally, the combination of Planck TT + lowP data with the Planck CMB lensing measurements provides a bound on neutrino masses of $\Sigma m_\nu < 1.64$ eV at 95% C.L. in the PCHIP case.

It can be noticed that in the PCHIP PPS there is a shift in the Hubble constant toward lower values. This occurs because there exists a strong, well-known degeneracy between the neutrino mass and the Hubble constant; see Fig. 6. In particular, considering CMB data only, a higher value of Σm_ν will shift the location of the angular diameter distance to the last scattering surface, a change that can be compensated with a smaller value of the Hubble constant H_0. The mean values of the clustering parameter σ_8 are also displaced by $\sim 2\sigma$ (except for the BAO case) toward lower values in the PCHIP PPS approach with respect to the mean values obtained when using the power-law PPS, as can be noticed from Fig. 7. Concerning the $P_{s,i}$ parameters, the bounds on $P_{s,i}$ with $i \geq 5$ are weaker with respect to the ΛCDM case (see Table I in the Appendix), and only the combination of Planck TT + lowP data with the MPkW measurements provides an upper limit for the $P_{s,12}$ (concretely, $P_{s,12} < 3.89$ at 95% C.L.).

Also, when considering the high-ℓ polarization measurements, the bounds on the sum of the neutrino masses are larger when using the PCHIP parametrization with

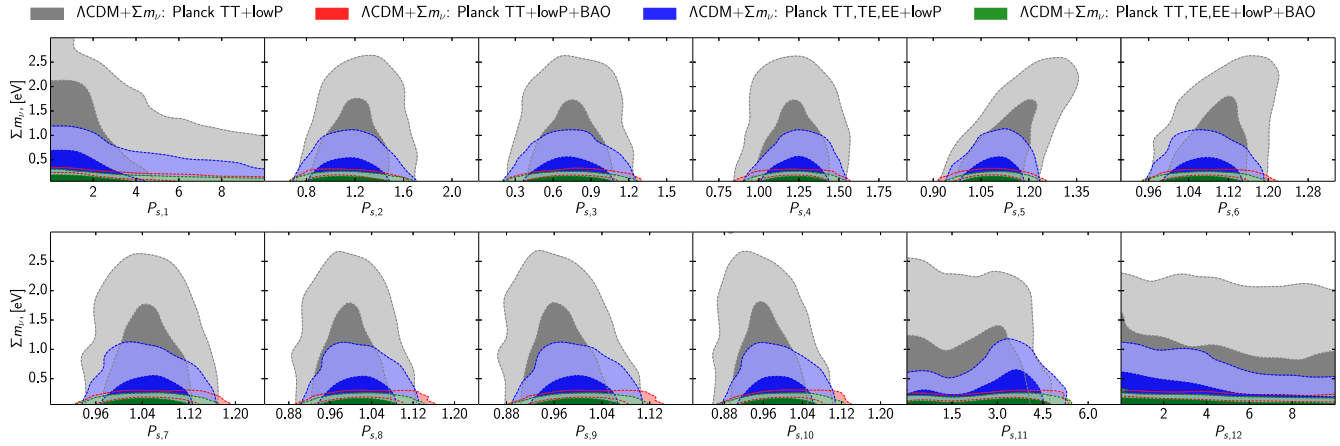

FIG. 5. As Fig. 3 but for the ΛCDM plus $\sum m_\nu$ case.

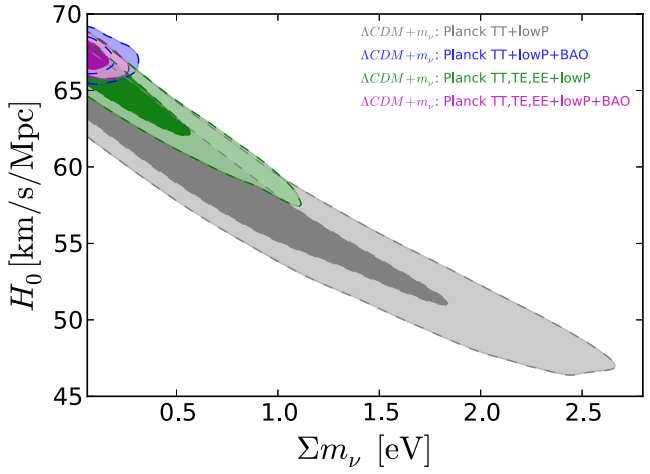

FIG. 6. 68% and 95% C.L. allowed regions in the (Σm_ν, H_0) plane, using different combinations of data sets, within the PCHIP PPS parametrization.

respect to the ones obtained with the power-law approach. However, these bounds are more stringent than those obtained using the Planck TT + lowP data only (see Table V in the Appendix). The reason for this improvement is due to the fact that the inclusion of the polarization measurements removes many of the degeneracies among the parameters. Concerning the CMB measurements only, we find an upper limit $\Sigma m_\nu < 0.880$ eV at 95% C.L. in the PCHIP approach. The addition of the matter power spectrum measurements leads to a value of $\Sigma m_\nu < 0.458$ eV at 95% C.L. in the PCHIP parametrization, improving the Planck TT, TE, EE + lowP constraint by a factor of 2. Notice that, as in the Planck TT + lowP results, the data combination that gives the most stringent constraints is the one involving the Planck TT, TE, EE + lowP and BAO data sets, since it provides a 95% C.L. upper bound on Σm_ν of 0.218 eV in the PCHIP PPS case. Finally, when the lensing measurements are added, the constraint on the neutrino masses is shifted to a higher value (agreeing with previous findings from the Planck collaboration), being $\Sigma m_\nu < 1.17$ eV at 95% C.L. for the PCHIP case. The degeneracies between Σm_ν and H_0, σ_8, even if milder than those without high-multipole polarization data, are still present (see Figs. 6 and 7). The constraints on the $P_{s,i}$ parameters do not differ much from those obtained with the Planck TT + lowP data.

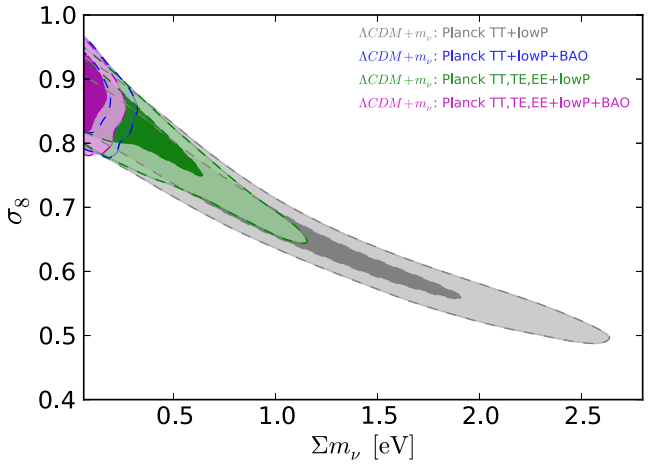

FIG. 7. 68% and 95% C.L. allowed regions in the (Σm_ν, σ_8) plane, using different combinations of data sets, within the PCHIP PPS parametrization.

VI. EFFECTIVE NUMBER OF RELATIVISTIC SPECIES AND NEUTRINO MASSES

After having analyzed the constraints on $N_{\rm eff}$ and Σm_ν separately, we study in this section their joint constraints in the context of the ΛCDM + $N_{\rm eff}$ + Σm_ν extended cosmological model, focusing mainly on the differences with the results presented in the two previous sections.

The 68% and 95% C.L. constraints on $N_{\rm eff}$ and Σm_ν are reported in Figs. 8 and 9, respectively, for different data set combinations and PPS choices; see also Tables VI and VII in the Appendix. Notice that the qualitative conclusions drawn in the previous sections do not change here. The PCHIP PPS parametrization still allows for a significant freedom in the values of $N_{\rm eff}$ and Σm_ν, as these parameters have an impact on the CMB spectrum that can be easily mimicked by some variations in the PPS nodes. In particular, a significant degeneracy between $N_{\rm eff}$ and the nodes $P_{s,6}$ to $P_{s,10}$ appears, in analogy to what happens in the ΛCDM + $N_{\rm eff}$ model (see Fig. 3 and the discussion in Sec. IV). At the same time, the strongest degeneracy involving the total neutrino mass appears between Σm_ν and $P_{s,5}$. This corresponds to a rescaling of the PPS that compensates the change in the early ISW contribution driven by massive neutrinos (see Fig. 5 and the discussion in Sec. V). We do not show here the degeneracies with the $P_{s,i}$ nodes for the ΛCDM + $N_{\rm eff}$ + Σm_ν model, but we

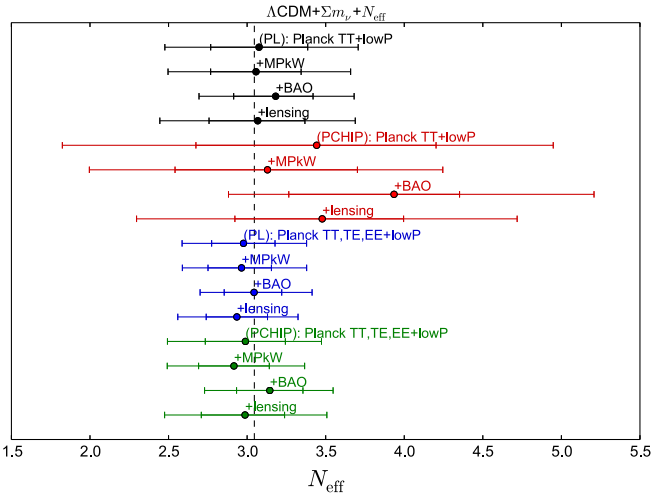

FIG. 8. As Fig. 2 but for the ΛCDM + $N_{\rm eff}$ + Σm_ν model.

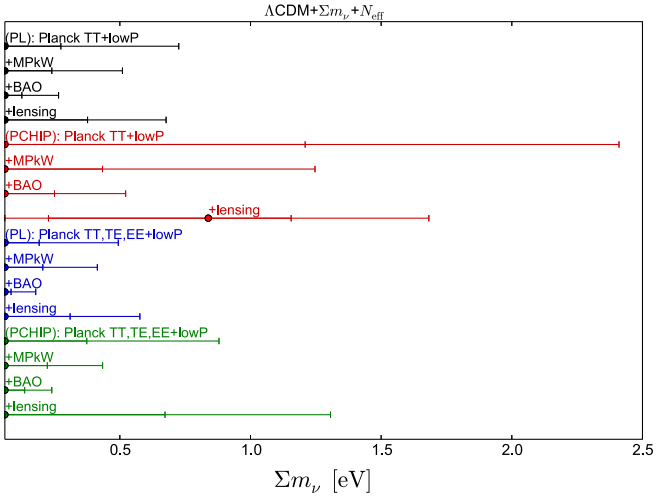

FIG. 9. As Fig. 8 but for the Σm_ν parameter.

have verified that they are qualitatively similar to those depicted in Fig. 3 (Fig. 5) for the $N_{\rm eff}$ (Σm_ν) parameter. When considering CMB data only, the constraints are slightly loosened with respect to those obtained when the $N_{\rm eff}$ and Σm_ν parameters are freely varied separately and not simultaneously. When comparing the power-law PPS and the PCHIP PPS models, we can notice that the variations of the neutrino parameters lead to several variations in other cosmological parameters. Such is the case of the baryon and CDM densities and the angular scale of the peaks, which are shifted by a significant amount, as a consequence of the degeneracies with both $N_{\rm eff}$ and Σm_ν. As the effects of $N_{\rm eff}$ and Σm_ν on the Hubble parameter H_0 and the clustering parameter σ_8 are opposite, we find an increased uncertainty in these parameters, indeed the allowed ranges for them are significantly enlarged.

While the tightest neutrino mass bound arises from the Planck TT + lowP + BAO data set, the largest allowed mean value for $N_{\rm eff}$ is also obtained for this very same data combination ($N_{\rm eff} = 3.94^{+0.42}_{-0.67}$ at 68% C.L. in the PCHIP PPS analysis), showing the large degeneracy between Σm_ν and $N_{\rm eff}$. However, when including the Planck CMB lensing measurements, the trend is opposite to the one observed with the BAO data set, with three times larger upper limits for Σm_ν and lower mean values for $N_{\rm eff}$. As stated before, the fact that lensing data prefer heavier neutrinos is well known (see, e.g., Sec. V and Refs. [39,65]). Notice, from Fig. 9, that the only combination which shows a preference for $\Sigma m_\nu > 0.06$ eV[2] at 68% C.L. includes the lensing data ($\Sigma m_\nu = 0.84^{+0.32}_{-0.62}$ eV, for the PCHIP PPS).

[2]This value roughly corresponds to the lower limit allowed by oscillation measurements if the total mass is distributed among the massive eigenstates according to the normal hierarchy scenario.

When polarization measurements are added in the data analyses, we obtain a 95% C.L. range of $2.5 \lesssim N_{\rm eff} \lesssim 3.5$, with very small differences in both the central values and allowed ranges for the several data combinations explored here; see Table VII in the Appendix. As in the ΛCDM + $N_{\rm eff}$ model, the data set including BAO data is the only one for which the mean value of $N_{\rm eff}$ is larger than 3, while in all the other cases it lies between 2.9 and 3. Apart from these small differences, all the results are perfectly in agreement with the standard value 3.046 within the 68% C.L. range. Concerning the Σm_ν parameter, the results are also very similar to those obtained in the ΛCDM + Σm_ν model illustrated in Sec. V, with only very small differences in the exact numerical values of the derived bounds. The most constraining results are always obtained with the inclusion of BAO data, from which we obtain $\Sigma m_\nu < 0.18(0.24)$ eV when using the power-law (PCHIP) PPS, both really close to the values derived in the ΛCDM + Σm_ν model.

For what concerns the remaining cosmological parameters, the differences between the power-law PPS and the PCHIP PPS results are much less significant when the polarization spectra are considered in the analyses. We may notice that the predicted values of the Hubble parameter H_0 are lower than the CMB estimates in the ΛCDM model, and consequently they show an even stronger tension with local measurements of the Hubble constant. This is due to the negative correlation between H_0 and Σm_ν. On the other hand, the ΛCDM + $N_{\rm eff}$ + Σm_ν model predicts a σ_8 smaller than what is obtained in the ΛCDM model for most of the data combinations, partially reconciling the CMB and the local estimates for this parameter.

The PCHIP nodes in this extended model do not deviate significantly from the expected values corresponding to the power-law PPS. The small deviations driven by the degeneracies with the neutrino parameters Σm_ν and $N_{\rm eff}$ are canceled by the stringent bounds set by the polarization spectra, which break these degeneracies. Deviations from the power-law expectations are still visible at small wave modes, corresponding to the dip at $\ell \simeq 20$ and to the small bump at $\ell \simeq 40$ in the CMB temperature spectrum.

VII. MASSIVE NEUTRINOS AND EXTRA MASSIVE STERILE NEUTRINO SPECIES

Standard cosmology includes as hot thermal relics the three light, active neutrino flavors of the Standard Model of elementary particles. However, the existence of extra hot relic components, as dark radiation relics, sterile neutrino species, and/or thermal axions is also possible. In their presence, the cosmological neutrino mass constraints will be changed. The existence of extra sub-eV massive sterile neutrino species is well motivated by the so-called short-baseline neutrino oscillation anomalies [52,66–68]. These extra light species have an associated free-streaming scale that will reduce the growth of matter fluctuations at small

scales. They also contribute to the effective number of relativistic degree of freedom (i.e., to $N_{\rm eff}$).

We explore in this section the ΛCDM scenario (in the two PPS parametrizations, power-law and PCHIP) with three active light massive neutrinos, plus one massive sterile neutrino species characterized by an effective mass $m_s^{\rm eff}$, which is defined by

$$m_s^{\rm eff} = \left(\frac{T_s}{T_\nu}\right)^3 m_s = (\Delta N_{\rm eff})^{3/4} m_s, \tag{6}$$

where T_s (T_ν) is the current temperature of the sterile (active) neutrino species, $\Delta N_{\rm eff} \equiv N_{\rm eff} - 3.046 = (T_s/T_\nu)^3$ is the effective number of degrees of freedom associated to the massive sterile neutrino, and m_s is its physical mass. For the numerical analyses, we use the following set of parameters to describe the model with a power-law PPS:

$$\{\Omega_b h^2, \Omega_c h^2, \theta, \tau, n_s, \log[10^{10} A_s], \Sigma m_\nu, N_{\rm eff}, m_s^{\rm eff}\}. \tag{7}$$

When considering the PCHIP PPS parametrization, n_s and A_s are replaced by the 12 parameters $P_{s,i}$ (with $i = 1, \ldots, 12$).

The 68% and 95% C.L. bounds on $m_s^{\rm eff}$ obtained with different data sets and PPS combinations are summarized in Fig. 10 and in Tables VIII and IX in the Appendix. Notice that, in general, the value of $N_{\rm eff}$ is larger than in the case in which the sterile neutrinos are considered massless (see Table II in the Appendix). As for the other extensions of the ΛCDM model we studied, the bounds on Σm_ν, $N_{\rm eff}$, and $m_s^{\rm eff}$ are weaker when considering the PCHIP PPS with respect to the ones obtained within the power-law PPS canonical scenario. Notice that the bounds on $m_s^{\rm eff}$ are not very stringent. This is due to the correlation between $m_s^{\rm eff}$ and $N_{\rm eff}$: sub-eV massive sterile neutrinos contribute to the matter energy density at recombination, and therefore a larger value of $N_{\rm eff}$ will be required to leave unchanged both the angular location and the height of the first acoustic peak of the CMB.

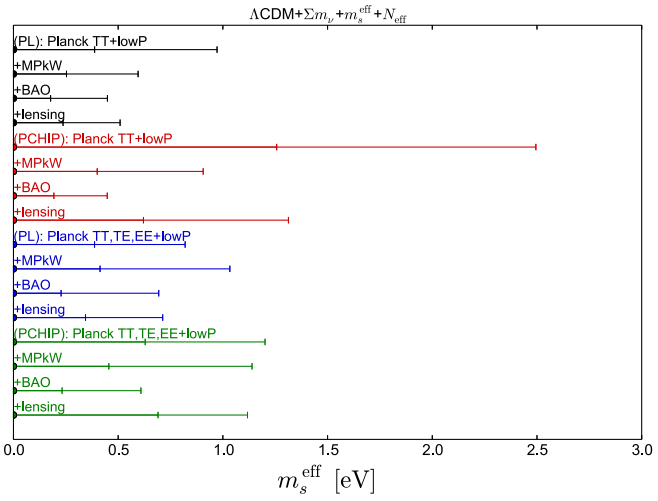

FIG. 10. 68% and 95% C.L. constraints on $m_s^{\rm eff}$, obtained in the $\Lambda{\rm CDM} + N_{\rm eff} + \Sigma m_\nu + m_s^{\rm eff}$ model. Different colors indicate Planck TT + lowP with PL PPS (black), Planck TT + lowP with PCHIP PPS (red), Planck TT, TE, EE + lowP with PL PPS (blue), and Planck TT, TE, EE + lowP with PCHIP PPS (green). For each color, we plot four different data sets: from top to bottom, we have CMB only, CMB + MPkW, CMB + BAO, and CMB + lensing.

Figure 11 illustrates the degeneracy between the active and the sterile neutrino masses. Since both active and sterile sub-eV massive neutrinos contribute to the matter energy density at decoupling, an increase of $m_s^{\rm eff}$ can be compensated by lowering Σm_ν, in order to keep fixed the matter content of the Universe. Notice that the most stringent 95% C.L. bounds on the three active and sterile neutrinos are obtained considering the BAO data in the two PPS cases. In particular, we find $\Sigma m_\nu < 0.481$ eV, $m_s^{\rm eff} < 0.448$ eV for the PCHIP parametrization and $\Sigma m_\nu < 0.263$ eV, $m_s^{\rm eff} < 0.449$ eV for the power-law approach. Furthermore, in general, when considering the PCHIP parametrization, the mean value on the Hubble constant is smaller than the value obtained in the standard power-law PPS framework, due to the strong degeneracy between Σm_ν and H_0. The value of the clustering parameter σ_8 is reduced in the two PPS parametrizations when comparing to the massless sterile neutrino case. This occurs because the sterile neutrino mass is another source of suppression of the large-scale structure growth.

The inclusion of the polarization data improves notably the constraints on the cosmological parameters in the model with a PCHIP parametrization. In particular, the neutrino constraints are stronger than those obtained using only the temperature power spectrum at small angular scales. This effect is related to the fact that many degeneracies are reduced by the high multipole polarization measurements (as, for example, the one between Σm_ν and τ). Concerning

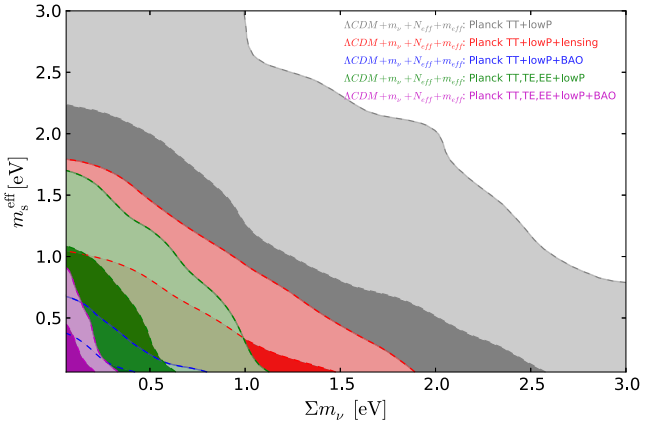

FIG. 11. 68% and 95% C.L. allowed regions in the (Σm_ν, $m_s^{\rm eff}$) plane using the different combination of data sets, within the PCHIP PPS parametrization.

the CMB measurements only, we find an upper limit on the three active and sterile neutrino masses of $\Sigma m_\nu < 0.83$ eV and $m_s^{\rm eff} < 1.20$ eV at 95% C.L., while for the effective number of relativistic degrees of freedom, we obtain $N_{\rm eff} < 3.67$ at 95% C.L., considering the PCHIP PPS approach. Also in this case, the most stringent constraints are obtained when adding the BAO data sets to the Planck TT,TE,EE +lowP data. Finally, the addition of the lensing potential displaces both the active and sterile neutrino mass constraints to higher values.

Concerning the $P_{s,i}$ parameters, we can notice that considering the Planck TT, TE, EE + lowP + BAO data sets, the dip corresponding to the $P_{s,3}$ node is reduced with respect to the other possible data combinations. We have an upper bound for the $P_{s,12}$ node from all the data combinations except for the CMB + lensing data set combination. In addition, as illustrated in Secs. V and VI, a significant degeneracy between $N_{\rm eff}$ and the nodes $P_{s,8}$ to $P_{s,10}$ and between Σm_ν and the nodes $P_{s,5}$ and $P_{s,6}$ is also present in this ΛCDM extension. Finally, because of the correlation between Σm_ν and $m_s^{\rm eff}$, degeneracies between $m_s^{\rm eff}$ and the nodes $P_{s,5}$ and $P_{s,6}$ will naturally appear.

VIII. THERMAL AXION

The axion field arises from the solution proposed by Peccei and Quinn [69–72] to solve the strong *CP* problem in QCD. They introduced a new global Peccei-Quinn symmetry $U(1)_{PQ}$ that, when spontaneously broken at an energy scale f_a, generates a pseudo-Nambu-Goldstone boson, the axion particle. Depending on the production process in the early Universe, thermal or nonthermal, the axion is a possible candidate for an extra hot thermal relic, together with the relic neutrino background, or for the cold dark matter component, respectively. In what follows, we shall focus on the thermal axion scenario. The axion coupling constant f_a is related to the thermal axion mass via

$$m_a = \frac{f_\pi m_\pi}{f_a}\frac{\sqrt{R}}{1+R} = 0.6\ \text{eV}\frac{10^7\ \text{GeV}}{f_a}, \tag{8}$$

with $R = 0.553 \pm 0.043$, the up-to-down quark masses ratio, and $f_\pi = 93$ MeV, the pion decay constant. Considering other values of R within the range 0.38–0.58 [73] does not affect in a significant way this relationship [74].

When the thermal axion is still a relativistic particle, it increases the effective number of relativistic degrees of freedom $N_{\rm eff}$, enhancing the amount of radiation in the early Universe; see Eq. (4). It is possible to compute the contribution of a thermal axion as an extra radiation component as

$$\Delta N_{\rm eff} = \frac{4}{7}\left(\frac{3}{2}\frac{n_a}{n_\nu}\right)^{4/3}, \tag{9}$$

with n_a the current axion number density and n_ν the present neutrino plus antineutrino number density per flavor. When the thermal axion becomes a nonrelativistic particle, it increases the amount of the hot dark matter density in the Universe, contributing to the total mass-energy density of the Universe. Thermal axions promote clustering only at large scales, suppressing the structure formation at scales smaller than their free-streaming scale, once the axion is a nonrelativistic particle. Several papers in the literature provide bounds on the thermal axion mass; see, for example, Refs. [63,75–80]. In this paper, our purpose is to update the work done in Ref. [35], in light of the recent Planck 2015 temperature and polarization data [32]. Therefore, in what follows, we present up-to-date constraints on the thermal axion mass, relaxing the assumption of a power-law for the PPS of the scalar perturbations, assuming also the PCHIP PPS scenario.

The bounds on the axion mass are relaxed in the PCHIP PPS scenario, as illustrated in Fig. 12 (see also Tables X and XI in the Appendix). This effect is related to the relaxed bound we have on $N_{\rm eff}$ when letting it free to vary in an extended ΛCDM + $N_{\rm eff}$ scenario. From the results presented in Table II, we find $N_{\rm eff} = 3.40^{+1.50}_{-1.43}$ at 95% C.L. for the PCHIP PPS parametrization, implying that the PCHIP formalism favors extra dark radiation, and therefore a higher axion mass will be allowed. As a consequence, we find that the axion mass is totally unconstrained using the Planck TT + lowP data in the PCHIP PPS approach. We instead find the bound $m_a < 1.97$ eV at 95% C.L. for the standard power-law case. The most stringent bounds arise when using the BAO data, since they are directly sensitive to the free-streaming nature of the thermal axion. While the MPkW measurements are also sensitive to this

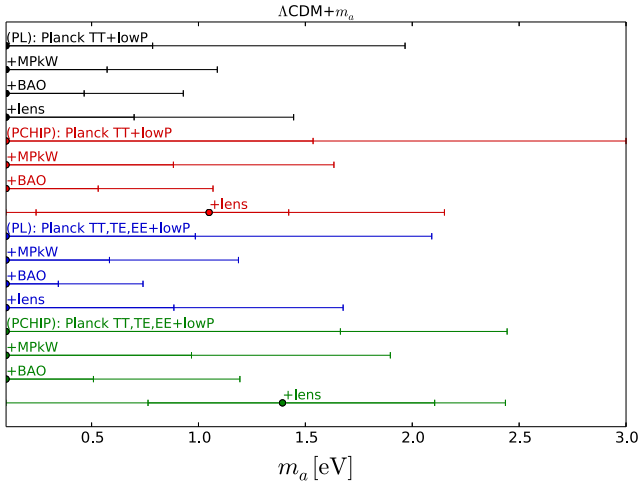

FIG. 12. As Fig. 2 but in the context of the ΛCDM + m_a model, focusing on the thermal axion mass m_a parameter.

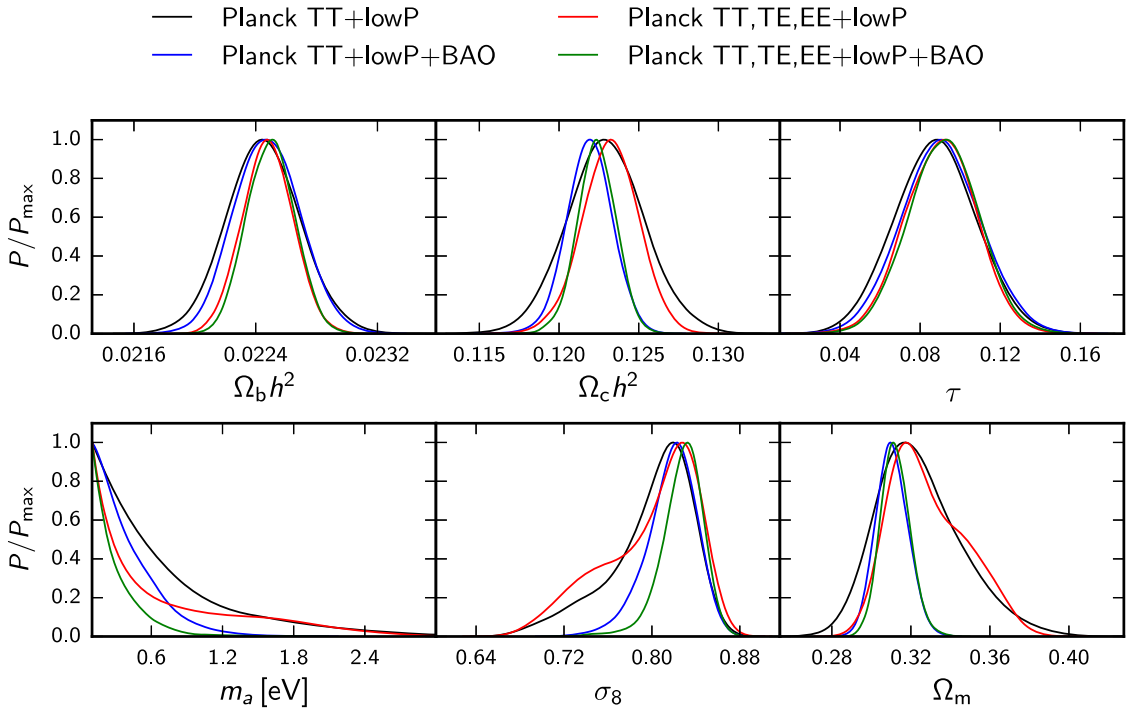

FIG. 13. One-dimensional posterior probability for some cosmological parameters for the combination of data sets labeled in the figure, for the power-law approach in the $\Lambda\mathrm{CDM} + m_a$ scenario.

small-scale structure suppression, BAO measurements are able to constrain better the cold dark matter density $\Omega_c h^2$, strongly correlated with m_a. We find $m_a < 0.93$ eV at 95% C.L. in the standard case and a slightly weaker constraint in the PCHIP case, $m_a < 1.07$ eV at 95% C.L. Finally, when considering the lensing data set, we obtain $m_a < 1.45$ eV at 95% C.L. in the power-law PPS case, a bound that is relaxed in the PCHIP PPS, $m_a < 2.15$ eV at 95% C.L. For this combination of data sets, a mild preference appears for an axion mass different from zero ($m_a = 1.05^{+0.37}_{-0.81}$ at 68% C.L.), only when considering the PCHIP approach, as illustrated in Fig. 12. This is probably due to the existing tension between the Planck lensing reconstruction data and the lensing effect; see Refs. [39,81].

The weakening of the axion mass constraints in most of the data combinations obtained in the PCHIP PPS scheme is responsible for the shift at more than 1σ in the cold dark matter mass-energy density, due to the existing degeneracy between m_a and $\Omega_c h^2$. Interestingly, this effect has also an impact on the Hubble constant, shifting its mean value by about 2σ toward lower values, similarly to the results obtained in the neutrino mass case. Furthermore, a shift in the optical depth toward a lower mean value is also present when analyzing the PCHIP PPS scenario. One can explain this shift via the existing degeneracies between τ and H_0 and between τ and $\Omega_c h^2$. Once BAO measurements are included in the data analyses, the degeneracies are, however, largely removed, and there is no significant shift in the values of the $\Omega_c h^2$, H_0, and τ parameters within the PCHIP PPS approach, when compared to their mean values in the power-law PPS. Concerning the $P_{s,i}$ parameters, we can observe also in this $\Lambda\mathrm{CDM} + m_a$ scenario a dip (corresponding to the $P_{s,3}$ node) and a bump (corresponding to the $P_{s,4}$ node); see Tables X and XI in the Appendix. These features are more significant for the case of CMB data only.

In general, the constraints arising from the addition of high-ℓ polarization measurements are slightly weaker than those previously obtained. The weakening of the axion mass is driven by the preference of Planck TT, TE, EE + lowP for a lower value of N_{eff}, as pointed out before. As shown in Ref. [35], the additional contribution to N_{eff} due to thermal axions is a steep function of the axion mass, at least for low thermal axion masses (i.e., below ~1 eV). The lower value of N_{eff} preferred by small-scale polarization dramatically sharpens the posterior of m_a at low mass (see Fig. 13). At higher masses, axions contribute mostly as cold dark matter; the posterior distribution flattens and overlaps with the one resulting from Planck TT + lowP, since CMB polarization does not help in improving the constraints on Ω_m (notice the presence of a bump in the posterior distributions of Ω_m and σ_8 for Planck TT,TE,EE+lowP). The mismatch in the values of Ω_m preferred by low and high thermal axion masses leads to a worsening in the constraints on m_a with respect to the Planck TT + lowP scenario, since the volume of the posterior distribution is now mainly distributed at higher

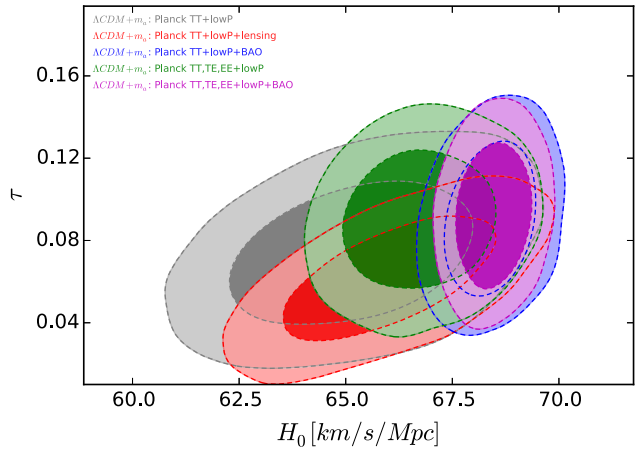

FIG. 14. 68% and 95% C.L. allowed regions in the (H_0, τ) plane using the different combinations of data sets in the $\Lambda\mathrm{CDM} + m_a$ model with a PCHIP PPS.

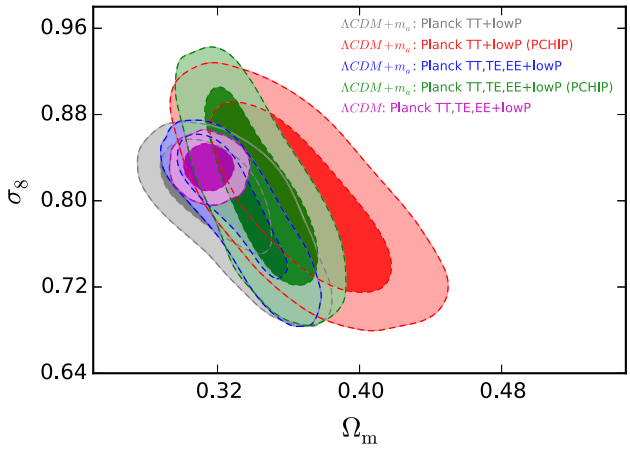

FIG. 15. 68% and 95% C.L. allowed regions in the (Ω_m, σ_8) plane using the different combinations of data sets in the $\Lambda\mathrm{CDM} + m_a$ model.

masses. When BAO data are considered, we get the tightest bounds on m_a. This is due to the fact that BAO measurements allow us to better constrain Ω_m, excluding the high-mass axion region. In addition, the bump in both the Ω_m and σ_8 distributions disappears completely, due to the higher constraining power on the clustering parameter and the matter density. As can be noticed from Fig. 13, the tail of the m_a distribution is excluded when adding BAO measurements.

Furthermore, the thermal axion mass bounds are relaxed within the PCHIP PPS formalism. In particular, concerning the CMB measurements only, $m_a < 2.44$ eV at 95% C.L. in the PCHIP approach, compared to the bound $m_a < 2.09$ eV at 95% C.L. in the standard power-law PPS description. When adding the MPkW we find upper limits on the axion mass that are $m_a < 1.19$ eV at 95% C.L. in the power-law PPS and $m_a < 1.90$ eV at 95% C.L. in the PCHIP parametrization. When considering the lensing data set, we obtain $m_a < 1.68$ eV at 95% C.L. in the power-law PPS case, which is relaxed in the PCHIP PPS, $m_a < 2.44$ eV at 95% C.L. A mild preference for an axion mass different from zero appears from this particular data combination ($m_a = 1.39^{+0.71}_{-0.63}$ at 68% C.L.) only when considering a PCHIP approach; see Fig. 12.

It is important to note that, when high-multipole polarization data are included, there is no shift induced in the mean value of the optical depth nor in the one corresponding to the cold dark matter energy density in the PCHIP approach (with respect to the power-law case). High-ℓ polarization data is extremely powerful in breaking degeneracies, as, for instance, the one existing between τ and H_0, as noticed from Fig. 14.

Interestingly, varying the thermal axion mass has a significant effect in the $\sigma_8 - \Omega_m$ plane in both PPS approaches, see Fig. 15, weakening the bounds found for the ΛCDM model and pushing the σ_8 (Ω_m) parameter toward a lower (higher) value. Concerning the $P_{s,i}$ parameters, the bounds on the nodes remain unchanged after adding the high-ℓ polarization data (when they are compared to the Planck TT + lowP baseline case). The significance of the dip and the bump are also very similar for the different data sets.

We have also explored the case in which both massive neutrinos and a thermal axion contribute as possible hot dark matter candidates. Our results, not illustrated here, show that the thermal axion mass bounds are unchanged in the extended $\Lambda\mathrm{CDM} + m_a + \Sigma m_\nu$ model with respect to the $\Lambda\mathrm{CDM} + m_a$ scenario, leading to almost identical axion mass contraints. On the other hand, the presence of thermal axions tightens the neutrino mass bounds, as these two thermal relics behave as hot dark matter with a free-streaming nature. The most stringent bounds on both the axion mass and on the total neutrino mass arise, as usual, from the addition of BAO data. We find $m_a < 1.18$ eV at 95% C.L. and $\Sigma m_\nu < 0.180$ eV at 95% C.L. in the PCHIP PPS when combining BAO with the Planck TT, TE,EE+lowP data sets.

IX. PRIMORDIAL POWER SPECTRUM RESULTS

From the MCMC analyses presented in the previous sections, we obtained constraints on the nodes used to parametrize the PCHIP PPS. Using this information, we can obtain a reconstruction of the spectrum shape for the different extensions of the ΛCDM model. Since the form of the reconstructed PPS is similar for the different models, we discuss now the common features of the PCHIP PPS as obtained for the ΛCDM model. We shall comment on the results for the data set combinations shown in Table I: Planck TT + lowP, Planck TT, TE, EE + lowP, Planck TT + lowP + MPkW, and

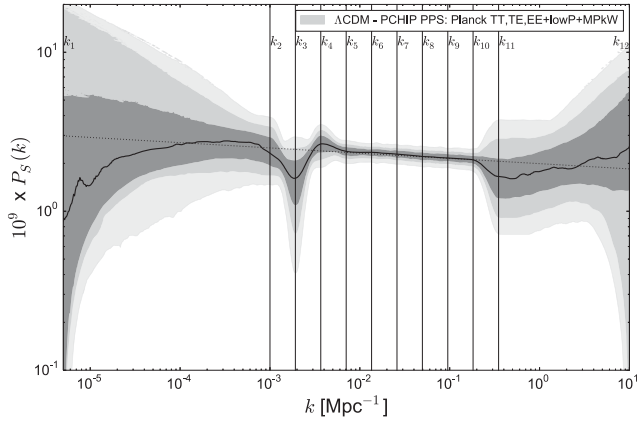

FIG. 16. Reconstruction of the marginalized best-fit PCHIP PPS (solid line) with 68%, 95%, and 99% confidence bands as obtained in the ΛCDM model, with the "'Planck TT, TE, EE + lowP + MPkW" data set. The dotted line represents the power-law PPS corresponding to the Planck best fit [39].

Planck TT, TE, EE + lowP + MPkW. Figure 16 illustrates the results for this last data set combination. For all data sets, the nodes $P_{s,1}$ and $P_{s,12}$ are badly constrained, due to the fact that these nodes are selected to cover a wide range of wave modes for computational reasons, but there are no available data to constrain them directly. Also, the node $P_{s,11}$ is not very well constrained by the Planck temperature data; however, the bounds on $P_{s,11}$ and $P_{s,12}$ can be improved with the inclusion of the high-multipole polarization data (TE,EE), leading to a significant improvement for $P_{s,11}$. The inclusion of the MPkW data allows us to further tighten the constraints on the last two nodes of the PCHIP PPS parametrization; see Fig. 16. The impact of the polarization on the nodes located at high k is smaller than the one due to the addition of the matter power spectrum data, since the MPkW data set provides very strong constraints on the smallest angular scales.

The bounds on the nodes at small wave modes ($P_{s,1}$ to $P_{s,4}$) are almost insensitive to the inclusion of additional data sets or to the change in the underlying cosmological model, with only small variations inside the 1σ range between the different results. The error bars on the nodes are larger in this part of the spectrum, since it corresponds to low multipoles in the CMB power spectra, where cosmic variance is larger. In this part of the PPS, we have the most evident deviations from the simple power-law PPS. The features are described by the node $P_{s,3}$, for which the value corresponding to the power-law PPS is approximately 2σ away from the reconstructed result, and by the node $P_{s,4}$, which is mildly discrepant with the power-law value (1σ level). These nodes describe the behavior of the CMB temperature spectrum at low ℓ, where the observations of the Planck and WMAP experiments show a lack of power at $\ell \simeq 20$ and an excess of power at $\ell \simeq 40$. The detection of these features is in agreement with several previous studies [16–29,34,35].[3]

The central part of the reconstructed PPS, from $P_{s,5}$ to $P_{s,10}$, is very well constrained by the data. In this range of wave modes, no deviations from the power-law PPS are visible, thus confirming the validity of the assumption that the PPS is almost scale invariant for a wide range of wave modes. This is also the region where the PPS shape is more sensitive to the changes in the ΛCDM model caused by its extensions.

As we can see from the results presented in previous sections, the constraints on the nodes $P_{s,5}$ to $P_{s,10}$ are different for each extension of the ΛCDM model, in agreement with the results obtained for $\ln[10^{10}A_s]$ and n_s when considering the power-law PPS. The value of the power-law PPS normalized to match the values of the PCHIP nodes can be calculated by means of the relation $P_s(k) = A_s(k/k_*)^{n_s-1}/P_0$: at each scale k, the value $P_s(k)$ is influenced both from A_s and n_s, since P_0 and k_* are fixed. In the various tables, when presenting the results on the power-law PPS, we listed the values of the PCHIP nodes that would correspond to the best-fitting A_s and n_s, to help in the comparison with the PCHIP PPS constraints. These values are calculated using Eq. (3). In the range between $k \simeq 0.007$ and $k \simeq 0.2$, the constraints in the PCHIP nodes correspond, for most of the cases, to the values expected by the power-law PPS analyses, within their allowed 1σ range. There are a few exceptions: for example, in the ΛCDM + $N_{\rm eff}$ model and with the Planck TT+lowP+BAO data set, the node $P_{s,10}$ deviates from the expected value corresponding to the power-law PPS by more than 1σ (see Table II). This is a consequence of the large correlation and the large variability range that this data set allows for $N_{\rm eff}$. A similar behavior appears in the ΛCDM + $N_{\rm eff}$ + Σm_ν model (see Table VI) and in the ΛCDM + Σm_ν + $N_{\rm eff}$ + $m_s^{\rm eff}$ model (Table VIII), for the same reasons. The inclusion of polarization data at high ℓ, limiting the range for $N_{\rm eff}$, does not allow for these deviations from the power-law PPS.

It is interesting to study how the previous findings depend on the choice of the PPS parametrization. One could ask then how many nodes are needed to capture hints for unexplored effects, which could be due to unaccounted for systematics or, more interestingly, to new physics. A number of nodes larger than the one explored here

[3]Since this behavior of the CMB spectrum at low multipoles has been reported by analyses of both Planck and WMAP data, it is unlikely that it is the consequence of some instrumental systematics. It is possible that this feature is simply the result of a large statistical fluctuation in a region of the spectrum where cosmic variance is very large. On the other hand, the lack of power at a precise scale can be the signal of some nonstandard inflationary mechanism that produced a nonstandard spectrum for the initial scalar perturbations. Future investigations will possibly clarify this aspect of the PPS.

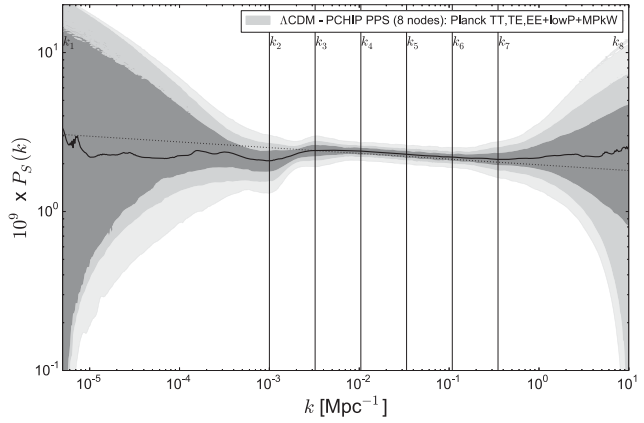

FIG. 17. Reconstruction of the marginalized best-fit PCHIP PPS (solid line) with 68%, 95%, and 99% confidence bands as obtained in the ΛCDM model, with the "'Planck TT, TE, EE + lowP + MPkW" data set, using a PCHIP parametrization with eight nodes for the PPS. The dotted line represents the power-law PPS corresponding to the Planck best fit [39].

(12 nodes) becomes unfeasible, as it would be extremely challenging computationally. However, lowering the number of nodes would be a very efficient solution for practical purposes, assuming the hints previously found are not totally diluted. We have therefore checked this alternative scenario, using eight nodes, as described in Sec. II B. The constraints on the PPS derived using this parametrization are reported in Fig. 17, obtained considering the ΛCDM model and the Planck TT, TE, EE + lowP + MPkW data set. The PCHIP parametrization with only eight nodes is not able to catch the features that are observed at $k \simeq 0.002$ Mpc^{-1} with 12 nodes, since there are not enough nodes at the relevant wave modes to describe the dip and the bump observed in the CMB spectrum. Having fewer nodes, the PPS can describe fewer features, it is more stable, and the behavior at small and high k can change. We found a preference for higher values for the node in $k_1^{(8)}$ than the one in k_1, as a consequence of the rules of the PCHIP function for fixing the first derivatives in the nodes. For the same reason, the constraints on the nodes in k_{11} and $k_7^{(8)}$ are slightly different, with a smaller preferred value for the eight-nodes case. We recall that the regions at extreme wave modes, however, are not well constrained by the experimental data. In the central region, where the CMB data are extremely precise, there is no difference between the two parametrizations. There is also no significant difference between the eight-nodes and the 12-nodes approaches when considering bounds on either the effective number of relativistic degrees of freedom $N_{\rm eff}$ or the total neutrino mass $\sum m_\nu$; in both cases, the cosmological constraints on $N_{\rm eff}$ and $\sum m_\nu$ get very close to the expected ones in the power-law PPS description after polarization measurements are included in the analyses; see the points obtained from the eight-nodes analysis case in Figs. 2 and 4.

To illustrate which PPS parametrization, among the three possible ones considered here, is preferred by current cosmological data, we compare, in the following, the minimum χ^2 resulting in each case from a fit to the Planck TT, TE, EE + lowP + MPkW data set. The minimum χ^2 for the power law, the PCHIP model with 12 nodes, and the PCHIP scenario with eight nodes are 13400, 13396, and 13392, respectively. The difference between the minimum χ^2 for the power-law approach and the PCHIP model with 12 nodes is $\Delta\chi^2 = 8$. These two models differ by ten parameters, which means that data prefer, albeit with a very poor statistical significance, the power-law PPS description. The same conclusion is reached when comparing instead the power-law and the PCHIP scenario with eight nodes. Therefore, though current cosmological data seem to prefer the power-law description, the statistical significance of this preference is still very mild, which may be sharpened by future measurements.

X. CONCLUSIONS

The description of the cosmological model may require a nonstandard power-law PPS of scalar perturbations generated during the inflationary phase at the beginning of the Universe. Several analyses have considered the possible deviations from the PPS power-law exploiting both the WMAP and the Planck data measurements of the CMB temperature power spectrum [16–29,34,35]. Even if the significance for such deviations is small, it leaves some freedom for the PPS assumed form. Here, we test the robustness of the cosmological bounds on several cosmological parameters when the PPS is allowed to have a model-independent shape, which we describe using a PCHIP function to interpolate a series of 12 or 8 nodes $P_{s,j}$.

We have explored the impact of a noncanonical PPS in several different extensions of the ΛCDM model, varying the effective number of relativistic species, the masses of the active and the light sterile neutrinos, the neutrino perturbations, and a thermal axion mass.

Concerning the effective number of degrees of freedom $N_{\rm eff}$, we find that the results are in good agreement with the standard value of 3.046, if one assumes the standard power-law PPS. Increasing $N_{\rm eff}$ has the main effect of increasing the Silk damping of the CMB spectrum at small scales, and therefore it is easy change the PPS shape at those scales to compensate the increased damping. This results in a strong degeneracy between the relevant PCHIP PPS nodes and $N_{\rm eff}$. As a consequence of volume effects in the Bayesian analyses, the constraints on $N_{\rm eff}$ are significantly loosened. For some data combinations, we obtain $N_{\rm eff} \simeq 4.8$ allowed at 95% C.L. However, the PCHIP PPS nodes and $N_{\rm eff}$ effects cannot be compensated in the polarization spectra, in particular in the case of the TE cross-correlation. This is the reason for which the inclusion of CMB polarization

measurements in the analyses allows us to break the degeneracies and to restore the $N_{\rm eff}$ bounds very close to 3.046 for all the data combinations, with $N_{\rm eff} > 3.5$ excluded at more than 95% C.L. for all the data sets.

In the minimal three active massive neutrinos scenario, the constraints on Σm_ν are relaxed with respect to the PPS power-law ones. This is due to the degeneracy between Σm_ν and the nodes $P_{s,5}$ and $P_{s,6}$, which correspond to the scales at which the early ISW effect contributes to the CMB spectrum. The tightest limit we find is $\Sigma m_\nu < 0.218$ eV at 95% C.L. from the combination of Planck TT, TE, EE + lowP + BAO data. The situation is not significantly changed when the effective number and the neutrino masses are varied simultaneously, since the degeneracies with the PPS parametrization are different for these two neutrino parameters. Their constraints are slightly relaxed as a consequence of the increased parameter space. The strongest bounds on Σm_ν arise from the Planck TT, TE, EE + lowP + BAO data set, for which we obtain $\Sigma m_\nu < 0.18$ eV (power-law PPS) and $\Sigma m_\nu < 0.24$ eV (PCHIP PPS). For $N_{\rm eff}$, all the data combinations including the Planck CMB polarization measurements give similar constraints, summarized as $2.5 \lesssim N_{\rm eff} \lesssim 3.5$ at 95% C.L.

In the case in which we consider both massive neutrinos and massive sterile neutrino species, the bounds on Σm_ν, $m_s^{\rm eff}$, and $N_{\rm eff}$ are weaker for the PCHIP approach when compared to the standard power-law PPS parametrization. This occurs because there exist degeneracies between these parameters and some nodes of the PCHIP PPS. The most stringent constraints on the active and the sterile neutrino parameters are obtained from the combination of Planck TT,TE,EE+lowP+BAO, for which we find $\Sigma m_\nu < 0.199$ eV, $m_s^{\rm eff} < 0.69$ eV, and $N_{\rm eff} < 3.41$ at 95% C.L. in the power-law PPS description and $\Sigma m_\nu < 0.219$ eV, $m_s^{\rm eff} < 0.61$ eV, and $N_{\rm eff} < 3.53$ at 95% C.L. within the PCHIP PPS parametrization.

Regarding the thermal axion scenario, we notice that the axion mass bounds are largely relaxed when using the PCHIP approach. When including the small-scale CMB polarization, we find a further weakening of the axion mass constraints: the reduced volume of the posterior distribution for small axion masses (m_a) is translated into a broadening of the marginalized constraints toward higher values for m_a. The strongest bound we find on the thermal axion mass within the PCHIP approach is $m_a < 1.07$ eV at 95% C.L. when considering the Planck TT + lowP + BAO data combination (while in the power-law scenario, $m_a < 0.74$ eV at 95% C.L.). Finally, when including massive neutrinos in addition to the thermal axions, we find that, while the bounds on the thermal axion mass are unaffected, the constraints on the total neutrino mass are tighter than those obtained without thermal axions. The strongest bounds we find for the thermal axion mass and the total neutrino mass in the PCHIP approach are $m_a < 1.03$ eV at 95% C.L. and $\Sigma m_\nu < 0.180$ eV at 95% C.L., when considering the Planck TT + lowP + BAO and Planck TT, TE, EE + lowP + BAO data set combinations, respectively. In the power-law PPS scenario, the strongest bounds are $m_a < 0.76$ eV at 95% C.L. and $\Sigma m_\nu < 0.159$ eV at 95% C.L., obtained for the Planck TT, TE, EE + lowP + BAO data set.

In summary, we have shown that degeneracies among the parameters involved in the ΛCDM model (and its possible extensions) and the PPS shape arise when considering CMB temperature power spectrum measurements only. Fortunately, these degeneracies disappear with the inclusion of high-ℓ polarization data. This is due to the fact that all these cosmological parameters influence the TT, TE, and EE spectra in different ways. This confirms the robustness of both the ΛCDM model and the simplest inflationary models, which predict a power-law PPS that successfully explains the observations at small scales. The large-scale fluctuations of the CMB spectrum, however, seem to point toward something new in the scenarios that describe inflation. It must be clarified whether these features are indicating a more complicated inflationary mechanism or are instead statistical fluctuations of the CMB temperature anisotropies.

Furthermore, we have as well verified that current data, albeit showing a very mild preference for the power-law scenario, is far from robustly discarding the PCHIP parametrization, and therefore future cosmological measurements are mandatory to sharpen the PPS profile.

ACKNOWLEDGMENTS

The work of S. G. and M. G. was supported by the Theoretical Astroparticle Physics research Grant No. 2012CPPYP7 under the Program PRIN 2012 funded by the Ministero dell'Istruzione, Università e della Ricerca. M. G. also acknowledges support by the Vetenskapsrådet (Swedish Research Council). This work has been done within the Labex ILP (reference ANR-10-LABX-63) part of the Idex SUPER and received financial state aid managed by the Agence Nationale de la Recherche, as part of the program Investissements d'Avenir under the reference ANR-11-IDEX-0004-02. E. D. V. acknowledges the support of the European Research Council via Grant No. 267117 (DARK, P. I. Joseph Silk). O. M. is supported by PROMETEO II/2014/050, by the Spanish Grant No. FPA2014-57816-P of the MINECO, by the MINECO Grant No. SEV-2014-0398, and by Grant No. PITN-GA-2011-289442-INVISIBLES.

APPENDIX: TABLES

See Tables I–XI.

TABLE I. The ΛCDM model: constraints on the cosmological parameters from the Planck TT + lowP and Planck TT, TE, EE + lowP data sets and also in combination with the matter power spectrum shape measurements from WiggleZ (MPkW), in the ΛCDM model (*nb* refers to *no bound*). For each combination, we report the limits obtained for the two parametrizations of the primordial power spectrum, namely, the power-law model (first column) and the polynomial expansion (second column of each data combination). Limits are at 95% C.L. around the mean value of the posterior distribution. For each data set, in the case of the power-law model, the values of $P_{s,i}$ are computed according to Eq. (3).

Parameter	Planck TT + lowP		Planck TT, TE, EE + lowP		Planck TT + lowP + MPkW		Planck TT, TE, EE + lowP + MPkW	
$\Omega_b h^2$	$0.02222^{+0.00045}_{-0.00043}$	$0.02175^{+0.00077}_{-0.00076}$	$0.02225^{+0.00032}_{-0.00030}$	$0.02215^{+0.00038}_{-0.00037}$	$0.02221^{+0.00044}_{-0.00045}$	$0.02190^{+0.00072}_{-0.00070}$	0.02223 ± 0.00031	$0.02214^{+0.00035}_{-0.00036}$
$\Omega_c h^2$	$0.1197^{+0.0043}_{-0.0042}$	$0.1231^{+0.0061}_{-0.0059}$	0.1198 ± 0.0029	$0.1209^{+0.0035}_{-0.0034}$	0.1198 ± 0.0039	$0.1223^{+0.0056}_{-0.0053}$	$0.1200^{+0.0028}_{-0.0027}$	0.1210 ± 0.0033
100θ	1.0409 ± 0.0009	1.0405 ± 0.0011	1.0408 ± 0.0006	1.0407 ± 0.0006	$1.0409^{+0.0009}_{-0.0010}$	1.0406 ± 0.0010	1.0408 ± 0.0006	1.0407 ± 0.0006
τ	$0.078^{+0.038}_{-0.036}$	$0.073^{+0.044}_{-0.042}$	0.079 ± 0.034	0.082 ± 0.040	$0.075^{+0.038}_{-0.039}$	$0.076^{+0.048}_{-0.046}$	$0.076^{+0.034}_{-0.033}$	$0.083^{+0.038}_{-0.037}$
n_S	0.966 ± 0.012	⋯	0.964 ± 0.010	⋯	0.965 ± 0.011	⋯	0.964 ± 0.009	⋯
$\ln[10^{10} A_s]$	$3.089^{+0.072}_{-0.069}$	⋯	3.094 ± 0.066	⋯	$3.084^{+0.073}_{-0.074}$	⋯	$3.087^{+0.066}_{-0.065}$	⋯
$H_0(\mathrm{km\,s^{-1}\,Mpc^{-1}})$	$67.3^{+1.9}_{-1.8}$	65.7 ± 2.7	67.3 ± 1.3	66.8 ± 1.5	$67.3^{+1.7}_{-1.8}$	66.1 ± 2.5	67.2 ± 1.2	$66.7^{+1.5}_{-1.4}$
σ_8	0.83 ± 0.03	0.87 ± 0.06	0.83 ± 0.03	$0.88^{+0.05}_{-0.06}$	0.83 ± 0.03	$0.84^{+0.04}_{-0.03}$	0.83 ± 0.03	0.83 ± 0.03
$P_{s,1}$	$\equiv 1.365$	< 7.93	$\equiv 1.397$	< 7.69	$\equiv 1.371$	< 7.90	$\equiv 1.388$	< 7.68
$P_{s,2}$	$\equiv 1.140$	$1.15^{+0.38}_{-0.35}$	$\equiv 1.155$	$1.14^{+0.39}_{-0.36}$	$\equiv 1.139$	$1.14^{+0.39}_{-0.36}$	$\equiv 1.147$	$1.14^{+0.38}_{-0.36}$
$P_{s,3}$	$\equiv 1.115$	$0.73^{+0.39}_{-0.37}$	$\equiv 1.128$	$0.71^{+0.38}_{-0.35}$	$\equiv 1.113$	$0.73^{+0.39}_{-0.38}$	$\equiv 1.120$	$0.72^{+0.38}_{-0.37}$
$P_{s,4}$	$\equiv 1.091$	$1.19^{+0.26}_{-0.25}$	$\equiv 1.102$	$1.22^{+0.23}_{-0.22}$	$\equiv 1.088$	1.19 ± 0.25	$\equiv 1.094$	1.22 ± 0.22
$P_{s,5}$	$\equiv 1.067$	1.07 ± 0.11	$\equiv 1.076$	$1.08^{+0.11}_{-0.10}$	$\equiv 1.063$	$1.07^{+0.12}_{-0.11}$	$\equiv 1.069$	1.08 ± 0.10
$P_{s,6}$	$\equiv 1.043$	$1.06^{+0.09}_{-0.08}$	$\equiv 1.051$	$1.07^{+0.08}_{-0.08}$	$\equiv 1.040$	1.06 ± 0.09	$\equiv 1.044$	$1.07^{+0.08}_{-0.07}$
$P_{s,7}$	$\equiv 1.021$	$1.04^{+0.09}_{-0.08}$	$\equiv 1.027$	1.04 ± 0.08	$\equiv 1.016$	1.03 ± 0.09	$\equiv 1.020$	$1.04^{+0.08}_{-0.07}$
$P_{s,8}$	$\equiv 0.998$	$0.99^{+0.09}_{-0.08}$	$\equiv 1.003$	1.01 ± 0.08	$\equiv 0.993$	1.00 ± 0.09	$\equiv 0.996$	$1.01^{+0.08}_{-0.07}$
$P_{s,9}$	$\equiv 0.976$	$0.97^{+0.09}_{-0.08}$	$\equiv 0.980$	$0.99^{+0.08}_{-0.07}$	$\equiv 0.971$	0.98 ± 0.09	$\equiv 0.973$	$0.99^{+0.08}_{-0.07}$
$P_{s,10}$	$\equiv 0.955$	$0.97^{+0.10}_{-0.09}$	$\equiv 0.957$	0.98 ± 0.09	$\equiv 0.949$	0.95 ± 0.09	$\equiv 0.951$	0.96 ± 0.08
$P_{s,11}$	$\equiv 0.934$	< 4.03	$\equiv 0.935$	$2.44^{+2.00}_{-2.37}$	$\equiv 0.928$	$0.82^{+0.45}_{-0.38}$	$\equiv 0.929$	$0.81^{+0.45}_{-0.38}$
$P_{s,12}$	$\equiv 0.833$	nb	$\equiv 0.829$	nb	$\equiv 0.825$	< 3.93	$\equiv 0.823$	< 3.44

TABLE II. Effective number of relativistic apecies: constraints on cosmological parameters from the Planck TT + lowP data set alone and in combination with the matter power spectrum shape measurements from WiggleZ (MPkW), the BAO data, and the lensing constraints from Planck, in the $\Lambda\mathrm{CDM} + N_{\mathrm{eff}}$ model (*nb* refers to *no bound*). For each combination, we report the limits obtained for the two parametrizations of the primordial power spectrum, namely, the power-law model (first column) and the polynomial expansion (second column of each pair). Limits are at 95% C.L. around the mean value of the posterior distribution. For each data set, in the case of power-law model, the values of $P_{s,i}$ are computed according to Eq. (3).

Parameter	Planck TT + lowP		Planck TT+lowP+MPkW		Planck TT+lowP+BAO		Planck TT+lowP+lensing	
$\Omega_b h^2$	$0.02230^{+0.00075}_{-0.00071}$	$0.02189^{+0.00107}_{-0.00105}$	$0.02221^{+0.00066}_{-0.00063}$	$0.02186^{+0.00081}_{-0.00082}$	0.02233 ± 0.00047	$0.02205^{+0.00060}_{-0.00057}$	$0.02232^{+0.00074}_{-0.00069}$	$0.02198^{+0.00093}_{-0.00091}$
$\Omega_c h^2$	$0.1205^{+0.0081}_{-0.0077}$	$0.1272^{+0.0189}_{-0.0182}$	$0.1198^{+0.0077}_{-0.0073}$	$0.1226^{+0.0148}_{-0.0141}$	$0.1207^{+0.0077}_{-0.0074}$	$0.1294^{+0.0153}_{-0.0146}$	$0.1195^{+0.0079}_{-0.0073}$	$0.1287^{+0.0169}_{-0.0161}$
100θ	1.0408 ± 0.0011	$1.0402^{+0.0019}_{-0.0018}$	1.0409 ± 0.0011	$1.0406^{+0.0017}_{-0.0016}$	1.0408 ± 0.0011	$1.0400^{+0.0015}_{-0.0014}$	1.0410 ± 0.0011	$1.0401^{+0.0017}_{-0.0015}$
τ	$0.080^{+0.044}_{-0.042}$	$0.076^{+0.050}_{-0.047}$	$0.075^{+0.040}_{-0.039}$	$0.075^{+0.048}_{-0.043}$	$0.082^{+0.035}_{-0.036}$	$0.079^{+0.046}_{-0.041}$	$0.069^{+0.040}_{-0.038}$	$0.066^{+0.042}_{-0.038}$
N_{eff}	$3.13^{+0.64}_{-0.63}$	$3.40^{+1.50}_{-1.43}$	$3.05^{+0.58}_{-0.54}$	$3.06^{+1.04}_{-1.00}$	$3.15^{+0.47}_{-0.44}$	$3.63^{+0.91}_{-0.80}$	$3.13^{+0.62}_{-0.61}$	$3.62^{+1.31}_{-1.19}$
n_S	$0.969^{+0.032}_{-0.030}$	…	$0.965^{+0.027}_{-0.026}$	…	$0.971^{+0.018}_{-0.017}$	…	$0.971^{+0.030}_{-0.028}$	…
$\ln[10^{10} A_s]$	$3.096^{+0.095}_{-0.089}$	…	$3.083^{+0.085}_{-0.084}$	…	$3.100^{+0.074}_{-0.075}$	…	$3.070^{+0.085}_{-0.079}$	…
$H_0(\mathrm{kms}^{-1}\mathrm{Mpc}^{-1})$	$68.0^{+5.7}_{-5.6}$	$68.2^{+11.4}_{-11.1}$	$67.3^{+4.8}_{-4.6}$	$66.0^{+7.4}_{-7.2}$	$68.3^{+3.0}_{-2.9}$	$70.2^{+4.6}_{-4.2}$	$68.5^{+5.6}_{-5.3}$	$70.2^{+9.4}_{-8.8}$
σ_8	$0.83^{+0.05}_{-0.04}$	$0.88^{+0.10}_{-0.09}$	0.83 ± 0.04	0.84 ± 0.06	0.84 ± 0.04	0.90 ± 0.08	0.82 ± 0.04	0.88 ± 0.08
$P_{s,1}$	$\equiv 1.337$	< 7.96	$\equiv 1.369$	< 7.97	$\equiv 1.318$	< 8.06	$\equiv 1.279$	< 7.87
$P_{s,2}$	$\equiv 1.135$	$1.14^{+0.40}_{-0.37}$	$\equiv 1.138$	$1.14^{+0.39}_{-0.36}$	$\equiv 1.130$	$1.14^{+0.41}_{-0.38}$	$\equiv 1.097$	$1.14^{+0.39}_{-0.37}$
$P_{s,3}$	$\equiv 1.112$	$0.73^{+0.41}_{-0.38}$	$\equiv 1.112$	$0.73^{+0.40}_{-0.37}$	$\equiv 1.109$	$0.72^{+0.41}_{-0.38}$	$\equiv 1.076$	$0.70^{+0.39}_{-0.37}$
$P_{s,4}$	$\equiv 1.090$	$1.20^{+0.27}_{-0.25}$	$\equiv 1.087$	1.19 ± 0.25	$\equiv 1.088$	$1.20^{+0.27}_{-0.26}$	$\equiv 1.056$	$1.18^{+0.26}_{-0.25}$
$P_{s,5}$	$\equiv 1.068$	$1.07^{+0.13}_{-0.12}$	$\equiv 1.062$	1.07 ± 0.11	$\equiv 1.068$	1.06 ± 0.12	$\equiv 1.036$	1.04 ± 0.10
$P_{s,6}$	$\equiv 1.047$	$1.06^{+0.10}_{-0.09}$	$\equiv 1.038$	$1.06^{+0.09}_{-0.08}$	$\equiv 1.048$	1.06 ± 0.09	$\equiv 1.017$	$1.03^{+0.07}_{-0.06}$
$P_{s,7}$	$\equiv 1.026$	$1.05^{+0.10}_{-0.09}$	$\equiv 1.015$	$1.03^{+0.09}_{-0.08}$	$\equiv 1.028$	$1.05^{+0.09}_{-0.08}$	$\equiv 0.998$	$1.02^{+0.08}_{-0.07}$
$P_{s,8}$	$\equiv 1.005$	$1.00^{+0.11}_{-0.10}$	$\equiv 0.992$	$1.00^{+0.10}_{-0.09}$	$\equiv 1.009$	1.02 ± 0.09	$\equiv 0.979$	0.99 ± 0.09
$P_{s,9}$	$\equiv 0.985$	$1.00^{+0.14}_{-0.13}$	$\equiv 0.970$	$0.97^{+0.11}_{-0.10}$	$\equiv 0.990$	1.02 ± 0.09	$\equiv 0.961$	$0.99^{+0.12}_{-0.11}$
$P_{s,10}$	$\equiv 0.965$	$1.01^{+0.20}_{-0.19}$	$\equiv 0.948$	$0.95^{+0.15}_{-0.14}$	$\equiv 0.972$	1.05 ± 0.12	$\equiv 0.943$	1.02 ± 0.17
$P_{s,11}$	$\equiv 0.946$	< 3.78	$\equiv 0.927$	$0.85^{+0.58}_{-0.45}$	$\equiv 0.954$	< 3.83	$\equiv 0.925$	< 3.55
$P_{s,12}$	$\equiv 0.853$	nb	$\equiv 0.824$	< 4.24	$\equiv 0.865$	nb	$\equiv 0.840$	nb

TABLE III. Effective number of relativistic species: constraints on cosmological parameters from Planck TT, TE, EE + lowP data set alone and in combination with the matter power spectrum shape measurements from WiggleZ (MPkW), the BAO data, and the lensing constraints from Planck, in the ΛCDM + $N_{\rm eff}$ model (*nb* refers to *no bound*). For each combination, we report the limits obtained for the two parametrizations of the primordial power spectrum, namely, the power-law model (first column) and the polynomial expansion (second column of each pair). Limits are at 95% C.L. around the mean value of the posterior distribution. For each data set, in the case of power-law model, the values of $P_{s,i}$ are computed according to Eq. (3).

Parameter	Planck TT, TE, EE + lowP		Planck TT,TE,EE+lowP+MPkW		Planck TT,TE,EE+lowP+BAO		Planck TT,TE,EE+lowP+lensing	
$\Omega_b h^2$	0.02220 ± 0.00048	$0.02206^{+0.00054}_{-0.00055}$	$0.02214^{+0.00047}_{-0.00046}$	0.02203 ± 0.00049	0.02229 ± 0.00038	$0.02226^{+0.00041}_{-0.00040}$	$0.02216^{+0.00045}_{-0.00046}$	$0.02204^{+0.00055}_{-0.00053}$
$\Omega_c h^2$	$0.1191^{+0.0062}_{-0.0061}$	$0.1197^{+0.0072}_{-0.0071}$	$0.1186^{+0.0062}_{-0.0061}$	$0.1191^{+0.0070}_{-0.0067}$	$0.1192^{+0.0060}_{-0.0059}$	$0.1203^{+0.0067}_{-0.0068}$	$0.1178^{+0.0058}_{-0.0057}$	$0.1184^{+0.0069}_{-0.0067}$
100θ	1.0409 ± 0.0009	$1.0408^{+0.0010}_{-0.0009}$	1.0409 ± 0.0009	1.0409 ± 0.0009	$1.0409^{+0.0009}_{-0.0008}$	1.0407 ± 0.0009	$1.0410^{+0.0009}_{-0.0008}$	$1.0410^{+0.0010}_{-0.0009}$
τ	0.077 ± 0.035	$0.081^{+0.040}_{-0.039}$	$0.073^{+0.036}_{-0.035}$	$0.080^{+0.039}_{-0.037}$	0.082 ± 0.032	0.087 ± 0.040	0.060 ± 0.028	$0.064^{+0.034}_{-0.032}$
$N_{\rm eff}$	$2.99^{+0.41}_{-0.39}$	$2.96^{+0.49}_{-0.48}$	$2.95^{+0.41}_{-0.39}$	$2.91^{+0.46}_{-0.43}$	3.04 ± 0.35	3.09 ± 0.40	2.94 ± 0.38	$2.92^{+0.48}_{-0.46}$
n_S	0.962 ± 0.019	⋯	0.960 ± 0.019	⋯	0.966 ± 0.015	⋯	$0.961^{+0.019}_{-0.018}$	⋯
$\ln[10^{10} A_s]$	3.088 ± 0.074	⋯	$3.078^{+0.075}_{-0.072}$	⋯	$3.098^{+0.067}_{-0.069}$	⋯	$3.049^{+0.058}_{-0.056}$	⋯
H_0(km s^{-1} Mpc^{-1})	$66.8^{+3.2}_{-3.1}$	$66.1^{+3.9}_{-3.8}$	66.5 ± 3.1	$65.8^{+3.6}_{-3.4}$	67.5 ± 2.4	$67.6^{+2.6}_{-2.5}$	66.7 ± 3.0	$66.2^{+3.9}_{-3.7}$
σ_8	$0.83^{+0.04}_{-0.03}$	0.87 ± 0.07	$0.82^{+0.04}_{-0.03}$	0.83 ± 0.04	0.83 ± 0.03	$0.88^{+0.06}_{-0.08}$	$0.81^{+0.03}_{-0.02}$	0.86 ± 0.06
$P_{s,1}$	$\equiv 1.415$	<7.62	$\equiv 1.427$	<7.79	$\equiv 1.377$	<7.27	$\equiv 1.373$	<8.15
$P_{s,2}$	$\equiv 1.157$	$1.14^{+0.38}_{-0.35}$	$\equiv 1.154$	$1.14^{+0.38}_{-0.35}$	$\equiv 1.150$	$1.14^{+0.38}_{-0.36}$	$\equiv 1.117$	$1.14^{+0.38}_{-0.35}$
$P_{s,3}$	$\equiv 1.128$	$0.72^{+0.37}_{-0.34}$	$\equiv 1.125$	$0.72^{+0.37}_{-0.35}$	$\equiv 1.125$	$0.73^{+0.38}_{-0.37}$	$\equiv 1.089$	$0.68^{+0.36}_{-0.34}$
$P_{s,4}$	$\equiv 1.101$	1.22 ± 0.22	$\equiv 1.096$	1.22 ± 0.22	$\equiv 1.100$	$1.23^{+0.22}_{-0.21}$	$\equiv 1.062$	1.20 ± 0.21
$P_{s,5}$	$\equiv 1.074$	1.08 ± 0.10	$\equiv 1.068$	$1.08^{+0.10}_{-0.09}$	$\equiv 1.076$	$1.09^{+0.11}_{-0.10}$	$\equiv 1.035$	$1.05^{+0.09}_{-0.08}$
$P_{s,6}$	$\equiv 1.048$	1.06 ± 0.08	$\equiv 1.040$	$1.06^{+0.08}_{-0.07}$	$\equiv 1.053$	$1.07^{+0.09}_{-0.08}$	$\equiv 1.009$	$1.03^{+0.07}_{-0.06}$
$P_{s,7}$	$\equiv 1.022$	1.04 ± 0.08	$\equiv 1.013$	$1.04^{+0.08}_{-0.07}$	$\equiv 1.030$	$1.05^{+0.09}_{-0.08}$	$\equiv 0.984$	1.00 ± 0.06
$P_{s,8}$	$\equiv 0.997$	$1.00^{+0.09}_{-0.08}$	$\equiv 0.987$	$1.00^{+0.08}_{-0.07}$	$\equiv 1.007$	$1.02^{+0.09}_{-0.08}$	$\equiv 0.959$	0.97 ± 0.07
$P_{s,9}$	$\equiv 0.973$	$0.98^{+0.09}_{-0.08}$	$\equiv 0.962$	$0.98^{+0.09}_{-0.08}$	$\equiv 0.985$	$1.00^{+0.09}_{-0.08}$	$\equiv 0.935$	0.95 ± 0.07
$P_{s,10}$	$\equiv 0.949$	$0.97^{+0.11}_{-0.10}$	$\equiv 0.937$	0.94 ± 0.10	$\equiv 0.964$	$1.00^{+0.11}_{-0.09}$	$\equiv 0.912$	$0.94^{+0.10}_{-0.09}$
$P_{s,11}$	$\equiv 0.926$	<4.30	$\equiv 0.913$	$0.77^{+0.42}_{-0.37}$	$\equiv 0.943$	$2.60^{+2.01}_{-2.52}$	$\equiv 0.889$	$2.57^{+1.96}_{-2.17}$
$P_{s,12}$	$\equiv 0.815$	nb	$\equiv 0.799$	<3.32	$\equiv 0.841$	nb	$\equiv 0.780$	nb

TABLE IV. Massive neutrinos: as Table II, but for the ΛCDM + Σm_ν model.

Parameter	Planck TT + lowP		Planck TT + lowP + MPkW		Planck TT + lowP + BAO		Planck TT + lowP + lensing	
$\Omega_b h^2$	$0.02214^{+0.00054}_{-0.00052}$	$0.02127^{+0.00097}_{-0.0010}$	$0.02217^{+0.00045}_{-0.00047}$	$0.02161^{+0.00089}_{-0.00103}$	$0.02228^{+0.00041}_{-0.00039}$	$0.02219^{+0.00063}_{-0.00061}$	$0.02210^{+0.00048}_{-0.00057}$	$0.02136^{+0.00081}_{-0.00079}$
$\Omega_c h^2$	$0.1202^{+0.0044}_{-0.0047}$	$0.1253^{+0.0067}_{-0.0064}$	$0.1200^{+0.0043}_{-0.0039}$	$0.1239^{+0.0072}_{-0.0067}$	$0.1188^{+0.0028}_{-0.0029}$	$0.1186^{+0.0032}_{-0.0033}$	$0.1197^{+0.0041}_{-0.0042}$	$0.1243^{+0.0060}_{-0.0059}$
100θ	$1.0407^{+0.0010}_{-0.0011}$	$1.03978^{+0.00137}_{-0.00136}$	$1.04076^{+0.00095}_{-0.00097}$	$1.04016^{+0.00131}_{-0.00146}$	$1.04098^{+0.00086}_{-0.00082}$	$1.04097^{+0.00084}_{-0.00081}$	$1.04078^{+0.00096}_{-0.00091}$	$1.03989^{+0.00118}_{-0.00112}$
τ	0.080 ± 0.038	$0.075^{+0.048}_{-0.044}$	$0.077^{+0.038}_{-0.037}$	$0.077^{+0.050}_{-0.043}$	$0.082^{+0.038}_{-0.037}$	$0.093^{+0.050}_{-0.047}$	$0.072^{+0.034}_{-0.032}$	$0.071^{+0.040}_{-0.037}$
Σm_ν(eV)	<0.754	<2.156	<0.455	<1.1497	<0.220	<0.261	<0.618	<1.636
n_S	$0.964^{+0.014}_{-0.013}$	…	0964 ± 0.012	…	0.968 ± 0.009	…	0.963 ± 0.014	…
$\ln[10^{10} A_s]$	$3.095^{+0.074}_{-0.073}$	…	$3.089^{+0.074}_{-0.070}$	…	3.096 ± 0.073	…	$3.077^{+0.061}_{-0.059}$	…
H_0(Km s^{-1} Mpc^{-1})	$65.5^{+5.9}_{-4.4}$	$58.4^{+8.8}_{-10.4}$	$66.3^{+3.2}_{-3.8}$	$62.4^{+6.3}_{-10.9}$	67.6 ± 1.3	$67.1^{+1.3}_{-1.4}$	$65.2^{+3.5}_{-3.8}$	$58.7^{+7.1}_{-6.8}$
σ_8	$0.794^{+0.110}_{-0.077}$	$0.715^{+0.182}_{-0.203}$	$0.809^{+0.055}_{-0.069}$	$0.771^{+0.104}_{-0.193}$	$0.825^{+0.039}_{-0.042}$	$0.869^{+0.067}_{-0.073}$	$0.772^{+0.054}_{-0.062}$	$0.7111^{+0.136}_{-0.142}$
$P_{s,1}$	$\equiv 1.399$	<8.23	$\equiv 1.390$	<7.81	$\equiv 1.349$	<8.08	$\equiv 1.386$	< 7.74
$P_{s,2}$	$\equiv 1.156$	$1.20^{+0.40}_{-0.36}$	$\equiv 1.149$	$1.17^{+0.38}_{-0.36}$	$\equiv 1.139$	$1.11^{+0.38}_{-0.34}$	$\equiv 1.140$	$1.21^{+0.37}_{-0.36}$
$P_{s,3}$	$\equiv 1.129$	$0.74^{+0.38}_{-0.37}$	$\equiv 1.122$	$0.74^{+0.38}_{-0.37}$	$\equiv 1.116$	$0.77^{+0.41}_{-0.40}$	$\equiv 1.113$	0.73 ± 0.39
$P_{s,4}$	$\equiv 1.103$	$1.22^{+0.28}_{-0.26}$	$\equiv 1.096$	1.20 ± 0.26	$\equiv 1.093$	1.21 ± 0.26	$\equiv 1.086$	1.23 ± 0.26
$P_{s,5}$	$\equiv 1.077$	$1.13^{+0.17}_{-0.15}$	$\equiv 1.071$	1.09 ± 0.13	$\equiv 1.070$	$1.08^{+0.13}_{-0.12}$	$\equiv 1.060$	1.11 ± 0.12
$P_{s,6}$	$\equiv 1.052$	$1.109^{+0.104}_{-0.097}$	$\equiv 1.046$	$1.080^{+0.090}_{-0.087}$	$\equiv 1.048$	$1.077^{+0.104}_{-0.100}$	$\equiv 1.035$	$1.076^{+0.075}_{-0.073}$
$P_{s,7}$	$\equiv 1.028$	$1.049^{+0.093}_{-0.087}$	$\equiv 1.022$	$1.044^{+0.091}_{-0.085}$	$\equiv 1.026$	$1.054^{+0.100}_{-0.093}$	$\equiv 1.010$	$1.034^{+0.069}_{-0.064}$
$P_{s,8}$	$\equiv 1.004$	$0.998^{+0.096}_{-0.085}$	$\equiv 0.998$	$1.002^{+0.098}_{-0.089}$	$\equiv 1.005$	$1.026^{+0.105}_{-0.100}$	$\equiv 0.986$	$0.988^{+0.076}_{-0.069}$
$P_{s,9}$	$\equiv 0.981$	$0.973^{+0.097}_{-0.084}$	$\equiv 0.975$	$0.977^{+0.098}_{-0.089}$	$\equiv 0.984$	$1.011^{+0.102}_{-0.097}$	$\equiv 0.963$	$0.966^{+0.077}_{-0.069}$
$P_{s,10}$	$\equiv 0.958$	$0.966^{+0.098}_{-0.095}$	$\equiv 0.953$	$0.956^{+0.097}_{-0.089}$	$\equiv 0.964$	$1.005^{+0.106}_{-0.096}$	$\equiv 0.940$	$0.968^{+0.085}_{-0.077}$
$P_{s,11}$	$\equiv 0.936$	$2.03^{+1.91}_{-2.02}$	$\equiv 0.930$	$0.97^{+1.77}_{-0.75}$	$\equiv 0.944$	$2.74^{+2.07}_{-2.69}$	$\equiv 0.918$	$2.74^{+1.53}_{-2.15}$
$P_{s,12}$	$\equiv 0.830$	nb	$\equiv 0.825$	< 3.89	$\equiv 0.848$	nb	$\equiv 0.811$	nb

TABLE V. Massive neutrinos: as Table III, but for the $\Lambda\mathrm{CDM} + \Sigma m_\nu$ model.

Parameter	Planck TT, TE, EE + lowP		Planck TT, TE, EE + lowP + MPkW		Planck TT, TE, EE + lowP + BAO		Planck TT, TE, EE + lowP + lensing	
$\Omega_b h^2$	$0.02221^{+0.00032}_{-0.00034}$	$0.022080^{+0.00039}_{-0.00040}$	$0.02223^{+0.00028}_{-0.00027}$	$0.02209^{+0.00037}_{-0.00038}$	0.022229 ± 0.00027	0.02226 ± 0.00033	0.02215 ± 0.00033	0.02203 ± 0.00041
$\Omega_c h^2$	$0.1200^{+0.0031}_{-0.0030}$	$0.1212^{+0.0035}_{-0.0034}$	$0.1199^{+0.0028}_{-0.0027}$	$0.1212^{+0.0035}_{-0.0033}$	0.1192 ± 0.0023	$0.1191^{+0.0024}_{-0.0025}$	0.1201 ± 0.0030	$0.1207^{+0.0033}_{-0.0035}$
100θ	$1.04068^{+0.00067}_{-0.00069}$	$1.0405^{+0.0069}_{-0.00071}$	$1.04072^{+0.00064}_{-0.00063}$	$1.04057^{+0.00065}_{-0.00069}$	$1.04083^{+0.00058}_{-0.00060}$	$1.04083^{+0.00058}_{-0.00059}$	$1.04063^{+0.00068}_{-0.00069}$	$1.04045^{+0.00072}_{-0.00073}$
τ	$0.081^{+0.033}_{-0.034} \pm 0.038$	$0.085^{+0.042}_{-0.040}$	0.080 ± 0.034	0.088 ± 0.037	$0.083^{+0.033}_{-0.032}$	$0.088^{+0.045}_{-0.040}$	$0.076^{+0.033}_{-0.032}$	0.082 ± 0.035
Σm_ν(eV)	< 0.497	< 0.880	< 0.349	< 0.458	< 0.175	< 0.218	< 0.625	< 1.172
n_S	$0.9638^{+0.0098}_{-0.0099}$	⋯	0.964 ± 0.009	⋯	0.966 ± 0.008	⋯	0.963 ± 0.009	⋯
$\ln[10^{10} A_s]$	$3.098^{+0.064}_{-0.065}$	⋯	$3.095^{+0.065}_{-0.066}$	⋯	$3.100^{+0.063}_{-0.064}$	⋯	$3.086^{+0.063}_{-0.061}$	⋯
$H_0(\mathrm{Km\,s^{-1}\,Mpc^{-1}})$	$66.3^{+2.9}_{-3.8}$	$64.3^{+3.9}_{-5.0}$	$66.7^{+2.3}_{-2.7}$	$64.4^{+2.1}_{-3.1}$	$67.5^{+1.1}_{-1.2}$	$67.1^{+1.3}_{-1.2}$	$65.0^{+3.3}_{-3.8}$	$62.8^{+5.1}_{-5.6}$
σ_8	$0.811^{+0.058}_{-0.076}$	$0.819^{+0.108}_{-0.136}$	$0.817^{+0.046}_{-0.055}$	$0.808^{+0.055}_{-0.064}$	$0.832^{+0.033}_{-0.034}$	$0.873^{+0.065}_{-0.076}$	$0.775^{+0.052}_{-0.062}$	$0.7117^{+0.116}_{-0.135}$
$P_{s,1}$	$\equiv 1.405$	< 7.52	$\equiv 1.399$	< 7.43	$\equiv 1.380$	< 7.59	$\equiv 1.399$	< 7.91
$P_{s,2}$	$\equiv 1.160$	$1.16^{+0.37}_{-0.35}$	$\equiv 1.156$	$1.15^{+0.40}_{-0.36}$	$\equiv 1.153$	$1.13^{+0.39}_{-0.36}$	$\equiv 1.150$	$1.18^{+0.38}_{-0.36}$
$P_{s,3}$	$\equiv 1.133$	$0.73^{+0.39}_{-0.36}$	$\equiv 1.129$	$0.73^{+0.39}_{-0.38}$	$\equiv 1.127$	$0.73^{+0.39}_{-0.37}$	$\equiv 1.123$	$0.73^{+0.37}_{-0.35}$
$P_{s,4}$	$\equiv 1.107$	$1.24^{+0.23}_{-0.22}$	$\equiv 1.103$	1.23 ± 0.23	$\equiv 1.103$	$1.23^{+0.23}_{-0.22}$	$\equiv 1.096$	1.24 ± 0.23
$P_{s,5}$	$\equiv 1.081$	1.10 ± 0.11	$\equiv 1.077$	1.10 ± 0.10	$\equiv 1.079$	$1.09^{+0.11}_{-0.10}$	$\equiv 1.070$	1.09 ± 0.11
$P_{s,6}$	$\equiv 1.056$	$1.073^{+0.091}_{-0.085}$	$\equiv 1.052$	$1.079^{+0.078}_{-0.073}$	$\equiv 1.055$	$1.069^{+0.093}_{-0.085}$	$\equiv 1.044$	$1.065^{+0.076}_{-0.072}$
$P_{s,7}$	$\equiv 1.031$	$1.050^{+0.086}_{-0.087}$	$\equiv 1.028$	$1.055^{+0.077}_{-0.072}$	$\equiv 1.032$	$1.046^{+0.092}_{-0.083}$	$\equiv 1.019$	$1.039^{+0.069}_{-0.068}$
$P_{s,8}$	$\equiv 1.007$	1.016 ± 0.084	$\equiv 1.004$	$1.021^{+0.077}_{-0.073}$	$\equiv 1.009$	$1.019^{+0.089}_{-0.088}$	$\equiv 0.995$	$1.007^{+0.070}_{-0.072}$
$P_{s,9}$	$\equiv 0.984$	$0.996^{+0.082}_{-0.081}$	$\equiv 0.981$	$0.998^{+0.075}_{-0.071}$	$\equiv 0.987$	$1.003^{+0.087}_{-0.079}$	$\equiv 0.972$	$0.988^{+0.068}_{-0.070}$
$P_{s,10}$	$\equiv 0.961$	$1.00^{+0.09}_{-0.08}$	$\equiv 0.958$	$0.97^{+0.9}_{-0.08}$	$\equiv 0.966$	$1.00^{+0.10}_{-0.09}$	$\equiv 0.948$	$0.98^{+0.08}_{-0.07}$
$P_{s,11}$	$\equiv 0.938$	$2.77^{+1.88}_{-2.63}$	$\equiv 0.936$	$0.82^{+0.56}_{-0.45}$	$\equiv 0.944$	$2.79^{+2.02}_{-2.72}$	$\equiv 0.926$	$3.015^{+1.51}_{-2.14}$
$P_{s,12}$	$\equiv 0.831$	nb	$\equiv 0.830$	< 3.20	$\equiv 0.843$	nb	$\equiv 0.818$	nb

TABLE VI. Effective number of relativistic species and neutrino masses: as Table II, but for the $\Lambda\mathrm{CDM} + N_{\mathrm{eff}} + \Sigma m_\nu$ model.

Parameter	Planck TT + lowP		Planck TT + lowP + MPkW		Planck TT + lowP + BAO		Planck TT + lowP + lensing	
$\Omega_b h^2$	$0.02215^{+0.00080}_{-0.00084}$	$0.02136^{+0.00125}_{-0.00112}$	$0.02215^{+0.00070}_{-0.00071}$	$0.02161^{+0.00095}_{-0.00109}$	$0.02236^{+0.00049}_{-0.00050}$	$0.02218^{+0.00065}_{-0.00061}$	$0.02212^{+0.00082}_{-0.00079}$	$0.02148^{+0.00097}_{-0.00089}$
$\Omega_c h^2$	$0.1205^{+0.0079}_{-0.0077}$	$0.1302^{+0.0200}_{-0.0214}$	$0.1203^{+0.0078}_{-0.0077}$	$0.1251^{+0.0156}_{-0.0150}$	$0.1207^{+0.0080}_{-0.0078}$	$0.1326^{+0.0192}_{-0.0165}$	$0.1201^{+0.0077}_{-0.0074}$	$0.1301^{+0.0169}_{-0.0172}$
100θ	$1.0407^{+0.0011}_{-0.0011}$	$1.0395^{+0.0021}_{-0.0020}$	$1.0407^{+0.0012}_{-0.0011}$	$1.0402^{+0.0018}_{-0.0017}$	$1.0408^{+0.0011}_{-0.0011}$	$1.0397^{+0.0015}_{-0.0016}$	$1.0407^{+0.0012}_{-0.0012}$	$1.0395^{+0.0018}_{-0.0017}$
τ	$0.081^{+0.043}_{-0.041}$	$0.075^{+0.047}_{-0.048}$	$0.078^{+0.044}_{-0.041}$	$0.076^{+0.049}_{-0.044}$	$0.085^{+0.039}_{-0.037}$	$0.084^{+0.048}_{-0.046}$	$0.076^{+0.042}_{-0.038}$	$0.074^{+0.043}_{-0.041}$
N_{eff}	$3.08^{+0.63}_{-0.60}$	$3.44^{+1.51}_{-1.62}$	$3.06^{+0.60}_{-0.56}$	$3.13^{+1.12}_{-1.13}$	$3.18^{+0.50}_{-0.49}$	$3.94^{+1.28}_{-1.05}$	$3.07^{+0.62}_{-0.62}$	$3.48^{+1.24}_{-1.18}$
$\Sigma m_\nu(\mathrm{eV})$	< 0.73	< 2.41	< 0.51	< 1.25	< 0.26	< 0.52	< 0.68	< 1.68
n_S	$0.965^{+0.032}_{-0.033}$	…	$0.964^{+0.029}_{-0.029}$	…	$0.973^{+0.021}_{-0.019}$	…	$0.965^{+0.033}_{-0.031}$	…
$\ln[10^{10}A_s]$	$3.098^{+0.093}_{-0.088}$	…	$3.091^{+0.094}_{-0.087}$	…	$3.106^{+0.084}_{-0.080}$	…	$3.085^{+0.089}_{-0.082}$	…
$H_0(\mathrm{km\,s^{-1}\,Mpc^{-1}})$	$65.8^{+7.6}_{-8.6}$	$60.5^{+14.2}_{-14.4}$	$65.9^{+5.9}_{-6.1}$	$62.9^{+10.0}_{-12.4}$	$68.3^{+3.0}_{-3.0}$	$71.2^{+5.7}_{-4.9}$	$65.3^{+7.3}_{-7.7}$	$61.6^{+10.5}_{-10.5}$
σ_8	$0.80^{+0.09}_{-0.12}$	$0.72^{+0.21}_{-0.21}$	$0.80^{+0.07}_{-0.08}$	$0.78^{+0.11}_{-0.18}$	$0.83^{+0.04}_{-0.05}$	$0.88^{+0.08}_{-0.08}$	$0.78^{+0.08}_{-0.09}$	$0.74^{+0.15}_{-0.16}$
$P_{s,1}$	$\equiv 1.390$	< 8.27	$\equiv 1.393$	< 7.99	$\equiv 1.302$	< 7.86	$\equiv 1.372$	< 7.85
$P_{s,2}$	$\equiv 1.155$	$1.20^{+0.41}_{-0.38}$	$\equiv 1.151$	$1.17^{+0.39}_{-0.37}$	$\equiv 1.128$	$1.14^{+0.42}_{-0.38}$	$\equiv 1.140$	$1.21^{+0.39}_{-0.37}$
$P_{s,3}$	$\equiv 1.129$	$0.73^{+0.39}_{-0.38}$	$\equiv 1.125$	$0.73^{+0.39}_{-0.37}$	$\equiv 1.109$	$0.73^{+0.42}_{-0.39}$	$\equiv 1.114$	$0.72^{+0.40}_{-0.37}$
$P_{s,4}$	$\equiv 1.103$	$1.22^{+0.28}_{-0.27}$	$\equiv 1.098$	$1.20^{+0.27}_{-0.26}$	$\equiv 1.089$	$1.21^{+0.27}_{-0.27}$	$\equiv 1.089$	$1.23^{+0.29}_{-0.27}$
$P_{s,5}$	$\equiv 1.078$	$1.13^{+0.18}_{-0.17}$	$\equiv 1.073$	$1.09^{+0.13}_{-0.13}$	$\equiv 1.070$	$1.06^{+0.13}_{-0.12}$	$\equiv 1.065$	$1.10^{+0.14}_{-0.12}$
$P_{s,6}$	$\equiv 1.054$	$1.09^{+0.11}_{-0.11}$	$\equiv 1.048$	$1.08^{+0.09}_{-0.09}$	$\equiv 1.052$	$1.06^{+0.10}_{-0.09}$	$\equiv 1.041$	$1.08^{+0.08}_{-0.07}$
$P_{s,7}$	$\equiv 1.030$	$1.05^{+0.10}_{-0.09}$	$\equiv 1.024$	$1.04^{+0.10}_{-0.09}$	$\equiv 1.033$	$1.06^{+0.10}_{-0.09}$	$\equiv 1.017$	$1.05^{+0.09}_{-0.08}$
$P_{s,8}$	$\equiv 1.007$	$1.00^{+0.11}_{-0.10}$	$\equiv 1.000$	$1.00^{+0.10}_{-0.10}$	$\equiv 1.015$	$1.03^{+0.10}_{-0.10}$	$\equiv 0.994$	$1.00^{+0.10}_{-0.09}$
$P_{s,9}$	$\equiv 0.985$	$0.99^{+0.13}_{-0.13}$	$\equiv 0.977$	$0.98^{+0.13}_{-0.12}$	$\equiv 0.998$	$1.04^{+0.11}_{-0.11}$	$\equiv 0.972$	$0.99^{+0.12}_{-0.11}$
$P_{s,10}$	$\equiv 0.962$	$1.01^{+0.20}_{-0.21}$	$\equiv 0.954$	$0.96^{+0.17}_{-0.16}$	$\equiv 0.980$	$1.09^{+0.16}_{-0.15}$	$\equiv 0.950$	$1.02^{+0.18}_{-0.18}$
$P_{s,11}$	$\equiv 0.941$	< 3.68	$\equiv 0.932$	$0.95^{+1.82}_{-0.74}$	$\equiv 0.963$	$2.21^{+1.75}_{-2.16}$	$\equiv 0.929$	$2.59^{+1.51}_{-1.96}$
$P_{s,12}$	$\equiv 0.837$	nb	$\equiv 0.826$	3.84	$\equiv 0.880$	nb	$\equiv 0.826$	nb

TABLE VII. Effective number of relativistic species and neutrino masses: as Table III, but for the $\Lambda\mathrm{CDM} + N_{\mathrm{eff}} + \Sigma m_\nu$ model.

Parameter	Planck TT, TE, EE + lowP		Planck TT, TE, EE + lowP + MPkW		Planck TT, TE, EE + lowP + BAO		Planck TT, TE, EE + lowP + lensing	
$\Omega_b h^2$	$0.02215^{+0.00049}_{-0.00050}$	$0.02202^{+0.00055}_{-0.00057}$	$0.02212^{+0.00049}_{-0.00048}$	$0.02200^{+0.00050}_{-0.00051}$	$0.02229^{+0.00038}_{-0.00037}$	$0.02233^{+0.00042}_{-0.00041}$	$0.02208^{+0.00048}_{-0.00048}$	$0.02196^{+0.00053}_{-0.00054}$
$\Omega_c h^2$	$0.1191^{+0.0062}_{-0.0059}$	$0.1204^{+0.0072}_{-0.0074}$	$0.1190^{+0.0064}_{-0.0058}$	$0.1194^{+0.0068}_{-0.0066}$	$0.1192^{+0.0062}_{-0.0057}$	$0.1206^{+0.0068}_{-0.0068}$	$0.1184^{+0.0060}_{-0.0057}$	$0.1200^{+0.0076}_{-0.0072}$
100θ	$1.0408^{+0.0009}_{-0.0009}$	$1.0406^{+0.0010}_{-0.0010}$	$1.0408^{+0.0009}_{-0.0009}$	$1.0408^{+0.0009}_{-0.0009}$	$1.0409^{+0.0008}_{-0.0008}$	$1.0407^{+0.0009}_{-0.0009}$	$1.0409^{+0.0009}_{-0.0009}$	$1.0405^{+0.0011}_{-0.0011}$
τ	$0.081^{+0.036}_{-0.036}$	$0.085^{+0.043}_{-0.041}$	$0.079^{+0.036}_{-0.035}$	$0.085^{+0.039}_{-0.038}$	$0.084^{+0.033}_{-0.034}$	$0.090^{+0.042}_{-0.042}$	$0.071^{+0.036}_{-0.034}$	$0.081^{+0.037}_{-0.037}$
N_{eff}	$2.98^{+0.40}_{-0.39}$	$2.99^{+0.48}_{-0.50}$	$2.96^{+0.41}_{-0.38}$	$2.92^{+0.45}_{-0.42}$	$3.04^{+0.37}_{-0.34}$	$3.14^{+0.40}_{-0.42}$	$2.93^{+0.39}_{-0.38}$	$2.99^{+0.52}_{-0.51}$
Σm_ν(eV)	< 0.50	< 0.88	< 0.41	< 0.44	< 0.18	< 0.24	< 0.58	< 1.31
n_S	$0.961^{+0.019}_{-0.020}$	⋯	$0.960^{+0.019}_{-0.018}$	⋯	$0.966^{+0.015}_{-0.015}$	⋯	$0.959^{+0.019}_{-0.019}$	⋯
$\ln[10^{10}A_s]$	$3.095^{+0.074}_{-0.075}$	⋯	$3.091^{+0.075}_{-0.074}$	⋯	$3.101^{+0.069}_{-0.072}$	⋯	$3.071^{+0.073}_{-0.069}$	⋯
$H_0(\mathrm{km\,s^{-1}\,Mpc^{-1}})$	$65.8^{+4.4}_{-4.9}$	$63.9^{+5.5}_{-5.7}$	$65.5^{+3.6}_{-4.0}$	$64.6^{+4.0}_{-4.3}$	$67.5^{+2.3}_{-2.3}$	$67.6^{+2.6}_{-2.6}$	$64.8^{+4.2}_{-4.6}$	$62.1^{+5.8}_{-5.7}$
σ_8	$0.81^{+0.07}_{-0.08}$	$0.82^{+0.11}_{-0.13}$	$0.80^{+0.05}_{-0.06}$	$0.80^{+0.06}_{-0.06}$	$0.83^{+0.04}_{-0.04}$	$0.88^{+0.07}_{-0.08}$	$0.78^{+0.06}_{-0.06}$	$0.76^{+0.11}_{-0.14}$
$P_{s,1}$	$\equiv 1.438$	< 8.11	$\equiv 1.445$	< 7.12	$\equiv 1.381$	< 7.82	$\equiv 1.253$	< 7.90
$P_{s,2}$	$\equiv 1.169$	$1.15^{+0.38}_{-0.35}$	$\equiv 1.169$	$1.16^{+0.37}_{-0.35}$	$\equiv 1.154$	$1.12^{+0.38}_{-0.35}$	$\equiv 1.081$	$1.17^{+0.38}_{-0.35}$
$P_{s,3}$	$\equiv 1.140$	$0.73^{+0.38}_{-0.37}$	$\equiv 1.139$	$0.72^{+0.38}_{-0.36}$	$\equiv 1.128$	$0.74^{+0.39}_{-0.37}$	$\equiv 1.061$	$0.72^{+0.38}_{-0.36}$
$P_{s,4}$	$\equiv 1.112$	$1.23^{+0.24}_{-0.23}$	$\equiv 1.110$	$1.23^{+0.23}_{-0.22}$	$\equiv 1.104$	$1.23^{+0.22}_{-0.22}$	$\equiv 1.042$	$1.24^{+0.24}_{-0.23}$
$P_{s,5}$	$\equiv 1.084$	$1.10^{+0.12}_{-0.11}$	$\equiv 1.081$	$1.09^{+0.10}_{-0.10}$	$\equiv 1.080$	$1.09^{+0.11}_{-0.10}$	$\equiv 1.023$	$1.10^{+0.12}_{-0.11}$
$P_{s,6}$	$\equiv 1.057$	$1.07^{+0.09}_{-0.08}$	$\equiv 1.054$	$1.07^{+0.08}_{-0.07}$	$\equiv 1.056$	$1.07^{+0.09}_{-0.09}$	$\equiv 1.005$	$1.06^{+0.08}_{-0.07}$
$P_{s,7}$	$\equiv 1.030$	$1.05^{+0.09}_{-0.08}$	$\equiv 1.027$	$1.05^{+0.08}_{-0.07}$	$\equiv 1.033$	$1.05^{+0.09}_{-0.09}$	$\equiv 0.986$	$1.04^{+0.07}_{-0.07}$
$P_{s,8}$	$\equiv 1.004$	$1.01^{+0.09}_{-0.08}$	$\equiv 1.000$	$1.01^{+0.08}_{-0.08}$	$\equiv 1.010$	$1.03^{+0.09}_{-0.09}$	$\equiv 0.969$	$1.00^{+0.08}_{-0.08}$
$P_{s,9}$	$\equiv 0.979$	$0.99^{+0.10}_{-0.09}$	$\equiv 0.975$	$0.98^{+0.09}_{-0.09}$	$\equiv 0.988$	$1.01^{+0.09}_{-0.09}$	$\equiv 0.951$	$0.98^{+0.09}_{-0.08}$
$P_{s,10}$	$\equiv 0.955$	$0.98^{+0.12}_{-0.11}$	$\equiv 0.949$	$0.95^{+0.10}_{-0.10}$	$\equiv 0.967$	$1.01^{+0.11}_{-0.11}$	$\equiv 0.934$	$0.98^{+0.11}_{-0.11}$
$P_{s,11}$	$\equiv 0.931$	$2.69^{+1.90}_{-2.62}$	$\equiv 0.925$	$0.78^{+0.55}_{-0.44}$	$\equiv 0.945$	$2.77^{+1.99}_{-2.67}$	$\equiv 0.917$	$3.00^{+1.49}_{-2.27}$
$P_{s,12}$	$\equiv 0.817$	nb	$\equiv 0.809$	< 2.98	$\equiv 0.844$	nb	$\equiv 0.835$	nb

TABLE VIII. massive neutrinos and extra massive sterile neutrino species: as Table II, but for the $\Lambda\mathrm{CDM} + \Sigma m_\nu + N_{\rm eff} + m_s^{\rm eff}$ model.

Parameter	Planck TT + lowP		Planck TT + lowP + MPkW		Planck TT + lowP + BAO		Planck TT + lowP + lensing	
$\Omega_b h^2$	$0.02229^{+0.00064}_{-0.00058}$	$0.02135^{+0.00103}_{-0.00095}$	$0.02228^{+0.00057}_{-0.00052}$	$0.02169^{+0.00088}_{-0.00098}$	$0.02252^{+0.00051}_{-0.00047}$	$0.02281^{+0.00066}_{-0.00062}$	$0.02230^{+0.00062}_{-0.00063}$	$0.02157^{+0.00090}_{-0.00087}$
$\Omega_c h^2$	$0.1217^{+0.0090}_{-0.0105}$	$0.1363^{+0.0171}_{-0.0158}$	$0.1209^{+0.0083}_{-0.0118}$	$0.1315^{+0.0149}_{-0.0144}$	0.1214 ± 0.0081	$0.1359^{+0.0210}_{-0.0195}$	$0.1226^{+0.0071}_{-0.0069}$	$0.1339^{+0.0152}_{-0.0139}$
100θ	$1.04039^{+0.00106}_{-0.00105}$	1.0399 ± 0.00170	$1.04048^{+0.00100}_{-0.00118}$	$1.03940^{+0.00151}_{-0.00161}$	$1.04064^{+0.00096}_{-0.00105}$	$1.03948^{+0.00161}_{-0.00158}$	$1.04040^{+0.00098}_{-0.00107}$	$1.03904^{+0.00139}_{-0.00148}$
τ	$0.088^{+0.043}_{-0.041}$	0.077 ± 0.046	$0.077^{+0.039}_{-0.038}$	$0.077^{+0.048}_{-0.046}$	$0.095^{+0.041}_{-0.040}$	$0.087^{+0.049}_{-0.045}$	0.084 ± 0.039	0.075 ± 0.043
Σm_ν(eV)	< 0.676	< 2.449	< 0.4778	< 1.167	< 0.263	< 0.481	< 0.641	< 1.385
$m_s^{\rm eff}$(eV)	< 0.972	< 2.495	< 0.898	< 0.906	< 0.449	< 0.448	< 0.509	< 1.313
$N_{\rm eff}$	< 3.638	< 4.917	< 3.616	< 4.404	< 3.762	< 5.466	< 3.661	< 4.623
n_S	$0.969^{+0.026}_{-0.022}$	…	$0.971^{+0.022}_{-0.019}$	…	$0.980^{+0.020}_{-0.018}$	…	$0.972^{+0.023}_{-0.022}$	…
$\ln[10^{10}A_s]$	$3.117^{+0.088}_{-0.082}$	…	$3.094^{+0.081}_{-0.075}$	…	3.129 ± 0.085	…	$3.108^{+0.080}_{-0.074}$	…
$H_0(\mathrm{Km\,s^{-1}\,Mpc^{-1}})$	$65.7^{+5.7}_{-6.1}$	$58.7^{+11.3}_{-11.4}$	$66.4^{+4.2}_{-4.1}$	$64.3^{+7.9}_{-9.9}$	$68.7^{+2.8}_{-2.4}$	$72.2^{+5.8}_{-5.4}$	$66.1^{+5.4}_{-5.7}$	$62.4^{+7.9}_{-8.3}$
σ_8	$0.782^{+0.095}_{-0.107}$	$0.632^{+0.217}_{-0.198}$	$0.771^{+0.058}_{-0.062}$	$0.753^{+0.118}_{-0.148}$	$0.807^{+0.051}_{-0.057}$	$0.866^{+0.081}_{-0.089}$	$0.771^{+0.057}_{-0.062}$	0.7191 ± 0.134
$P_{s,1}$	$\equiv 1.365$	< 7.78	$\equiv 1.310$	< 7.78	$\equiv 1.249$	< 7.55	$\equiv 1.316$	< 8.25
$P_{s,2}$	$\equiv 1.159$	$1.25^{+0.41}_{-0.39}$	$\equiv 1.123$	$1.20^{+0.41}_{-0.38}$	$\equiv 1.123$	$1.14^{+0.41}_{-0.38}$	$\equiv 1.135$	$1.22^{+0.42}_{-0.38}$
$P_{s,3}$	$\equiv 1.135$	$0.74^{+0.40}_{-0.38}$	$\equiv 1.102$	$0.72^{+0.41}_{-0.38}$	$\equiv 1.109$	$0.73^{+0.42}_{-0.40}$	$\equiv 1.114$	0.73 ± 0.41
$P_{s,4}$	$\equiv 1.113$	$1.23^{+0.30}_{-0.28}$	$\equiv 1.082$	$1.22^{+0.28}_{-0.27}$	$\equiv 1.094$	$1.24^{+0.28}_{-0.27}$	$\equiv 1.094$	1.23 ± 0.28
$P_{s,5}$	$\equiv 1.091$	$1.08^{+0.19}_{-0.18}$	$\equiv 1.062$	$1.09^{+0.14}_{-0.13}$	$\equiv 1.080$	$1.07^{+0.13}_{-0.12}$	$\equiv 1.074$	1.112 ± 0.13
$P_{s,6}$	$\equiv 1.069$	$1.122^{+0.121}_{-0.119}$	$\equiv 1.042$	$1.078^{+0.094}_{-0.086}$	$\equiv 1.066$	$1.058^{+0.102}_{-0.094}$	$\equiv 1.055$	$1.084^{+0.083}_{-0.076}$
$P_{s,7}$	$\equiv 1.047$	$1.071^{+0.092}_{-0.093}$	$\equiv 1.022$	$1.053^{+0.092}_{-0.087}$	$\equiv 1.052$	$1.069^{+0.100}_{-0.091}$	$\equiv 1.036$	$1.058^{+0.086}_{-0.079}$
$P_{s,8}$	$\equiv 1.027$	1.022 ± 0.096	$\equiv 1.003$	$1.012^{+0.098}_{-0.091}$	$\equiv 1.039$	$1.040^{+0.104}_{-0.098}$	$\equiv 1.017$	$1.013^{+0.092}_{-0.089}$
$P_{s,9}$	$\equiv 1.006$	$1.015^{+0.108}_{-0.107}$	$\equiv 0.984$	$1.003^{+0.108}_{-0.100}$	$\equiv 1.025$	$1.058^{+0.117}_{-0.110}$	$\equiv 0.999$	$1.012^{+0.107}_{-0.103}$
$P_{s,10}$	$\equiv 0.986$	$1.06^{+0.16}_{-0.15}$	$\equiv 0.966$	$1.02^{+0.14}_{-0.13}$	$\equiv 1.012$	$1.12^{+0.17}_{-0.16}$	$\equiv 0.981$	$1.06^{+0.15}_{-0.14}$
$P_{s,11}$	$\equiv 0.966$	< 3.49	$\equiv 0.948$	$1.10^{+1.31}_{-0.85}$	$\equiv 0.999$	$2.29^{+1.72}_{-2.15}$	$\equiv 0.963$	$2.66^{+1.43}_{-1.77}$
$P_{s,12}$	$\equiv 0.871$	nb	$\equiv 0.860$	< 3.82	$\equiv 0.934$	nb	$\equiv 0.877$	nb

TABLE IX. Massive neutrinos and extra massive sterile neutrino species: as Table III, but for the $\Lambda\mathrm{CDM} + \Sigma m_\nu + N_{\mathrm{eff}} + m_s^{\mathrm{eff}}$ model.

Parameter	Planck TT, TE, EE + lowP		Planck TT, TE, EE + lowP + MPkW		Planck TT, TE, EE + lowP + BAO		Planck TT, TE, EE + lowP + lensing	
$\Omega_b h^2$	$0.02286^{+0.00037}_{-0.00036}$	0.02226 ± 0.00046	$0.02226^{+0.00036}_{-0.00038}$	$0.02184^{+0.00041}_{-0.00039}$	$0.02241^{+0.00036}_{-0.00032}$	$0.02242^{+0.00041}_{-0.00038}$	$0.02227^{+0.00037}_{-0.00036}$	$0.02226^{+0.00049}_{-0.00047}$
$\Omega_c h^2$	$0.1207^{+0.0061}_{-0.0071}$	$0.1223^{+0.0074}_{-0.0076}$	$0.1189^{+0.0080}_{-0.0099}$	$0.1203^{+0.0083}_{-0.0110}$	$0.1189^{+0.0068}_{-0.0081}$	$0.1201^{+0.0077}_{-0.0079}$	$0.1207^{+0.0064}_{-0.0070}$	$0.1228^{+0.0068}_{-0.0063}$
100θ	$1.04043^{+0.00071}_{-0.00074}$	$1.040217^{+0.00078}_{-0.00084}$	$1.04048^{+0.00070}_{-0.00073}$	$1.04038^{+0.00073}_{-0.00079}$	$1.04070^{+0.00066}_{-0.00071}$	$1.04058^{+0.00073}_{-0.00081}$	$1.04046^{+0.00069}_{-0.00075}$	$1.04009^{+0.00085}_{-0.00084}$
τ	$0.087^{+0.035}_{-0.036}$	$0.090^{+0.044}_{-0.043}$	$0.084^{+0.034}_{-0.033}$	$0.088^{+0.040}_{-0.039}$	0.089 ± 0.034	$0.092^{+0.042}_{-0.043}$	$0.079^{+0.034}_{-0.031}$	$0.0083^{+0.036}_{-0.037}$
Σm_ν(eV)	< 0.528	< 0.829	< 0.365	< 0.401	< 0.199	< 0.219	< 0.573	< 1.071
m_s^{eff}(eV)	< 0.820	< 1.201	< 1.033	< 1.139	< 0.694	< 0.609	< 0.713	< 1.118
N_{eff}	< 3.410	< 3.669	< 3.374	< 3.440	< 3.405	< 3.527	< 3.405	< 3.698
n_S	0.965 ± -0.013	⋯	$0.975^{+0.014}_{-0.012}$	⋯	$0.970^{+0.014}_{-0.013}$	⋯	$0.965^{+0.014}_{-0.013}$	⋯
$\ln[10^{10} A_s]$	$3.115^{+0.071}_{-0.070}$	⋯	$3.107^{+0.070}_{-0.066}$	⋯	$3.114^{+0.068}_{-0.070}$	⋯	$3.097^{+0.066}_{-0.061}$	⋯
$H_0(\mathrm{Km\,s^{-1}\,Mpc^{-1}})$	$65.5^{+3.2}_{-3.7}$	$64.2^{+4.2}_{-5.0}$	$66.1^{+2.4}_{-2.7}$	$65.5^{+2.6}_{-3.1}$	$67.4^{+1.8}_{-1.6}$	$67.8^{+2.1}_{-1.8}$	$65.2^{+3.2}_{-3.8}$	$63.1^{+4.7}_{-5.3}$
σ_8	$0.768^{+0.077}_{-0.087}$	$0.761^{+0.126}_{-0.125}$	$0.781^{+0.060}_{-0.063}$	$0.778^{+0.071}_{-0.072}$	$0.806^{+0.048}_{-0.054}$	$0.856^{+0.076}_{-0.083}$	$0.754^{+0.063}_{-0.067}$	$0.723^{+0.113}_{-0.105}$
$P_{s,1}$	$\equiv 1.414$	< 7.52	$\equiv 1.279$	< 8.02	$\equiv 1.349$	< 7.76	$\equiv 1.389$	< 6.62
$P_{s,2}$	$\equiv 1.175$	$1.17^{+0.37}_{-0.36}$	$\equiv 1.120$	$1.15^{+0.39}_{-0.36}$	$\equiv 1.151$	$1.12^{+0.39}_{-0.35}$	$\equiv 1.154$	$1.21^{+0.38}_{-0.36}$
$P_{s,3}$	$\equiv 1.148$	$0.73^{+0.40}_{-0.38}$	$\equiv 1.102$	$0.73^{+0.38}_{-0.36}$	$\equiv 1.128$	$0.75^{+0.40}_{-0.38}$	$\equiv 1.128$	$0.71^{+0.39}_{-0.36}$
$P_{s,4}$	$\equiv 1.122$	$1.26^{+0.25}_{-0.23}$	$\equiv 1.085$	1.23 ± 0.22	$\equiv 1.107$	1.23 ± 0.23	$\equiv 1.102$	$1.25^{+0.25}_{-0.23}$
$P_{s,5}$	$\equiv 1.097$	1.12 ± 0.12	$\equiv 1.067$	1.10 ± 0.11	$\equiv 1.085$	1.10 ± 0.11	$\equiv 1.077$	1.11 ± 0.11
$P_{s,6}$	$\equiv 1.072$	$1.070^{+0.100}_{-0.094}$	$\equiv 1.050$	$1.072^{+0.086}_{-0.084}$	$\equiv 1.064$	$1.075^{+0.093}_{-0.085}$	$\equiv 1.053$	$1.077^{+0.074}_{-0.075}$
$P_{s,7}$	$\equiv 1.048$	$1.060^{+0.095}_{-0.089}$	$\equiv 1.033$	$1.058^{+0.081}_{-0.081}$	$\equiv 1.044$	1.054 ± 0.090	$\equiv 1.029$	1.04 ± 0.070
$P_{s,8}$	$\equiv 1.024$	$1.0033^{+0.094}_{-0.093}$	$\equiv 1.016$	$1.026^{+0.084}_{-0.084}$	$\equiv 1.023$	1.032 ± 0.090	$\equiv 1.006$	$1.018^{+0.075}_{-0.073}$
$P_{s,9}$	$\equiv 1.001$	$1.016^{+0.095}_{-0.093}$	$\equiv 1.000$	$1.004^{+0.086}_{-0.085}$	$\equiv 1.004$	1.020 ± 0.090	$\equiv 0.984$	$1.004^{+0.078}_{-0.074}$
$P_{s,10}$	$\equiv 0.979$	$1.02^{+0.11}_{-0.11}$	$\equiv 0.984$	0.98 ± 0.10	$\equiv 0.984$	1.02 ± 0.11	$\equiv 0.961$	$1.01^{+0.10}_{-0.09}$
$P_{s,11}$	$\equiv 0.957$	$2.87^{+1.59}_{-2.55}$	$\equiv 0.968$	$0.83^{+0.71}_{-0.57}$	$\equiv 0.965$	$2.95^{+1.94}_{-2.76}$	$\equiv 0.940$	$3.28^{+1.39}_{-1.29}$
$P_{s,12}$	$\equiv 0.851$	< 8.49	$\equiv 0.890$	< 2.60	$\equiv 0.873$	< 8.59	$\equiv 0.836$	nb

TABLE X. Thermal axion: as Table II, but for the ΛCDM + m_a model.

Parameter	Planck TT + lowP		Planck TT + lowP + MPkW		Planck TT + lowP + BAO		Planck TT + lowP + lensing	
$\Omega_b h^2$	$0.02245^{+0.00048}_{-0.00046}$	$0.02178^{+0.00080}_{-0.00079}$	$0.02240^{+0.00045}_{-0.00043}$	$0.02191^{+0.00074}_{-0.00071}$	$0.02248^{+0.00043}_{-0.00040}$	$0.02224^{+0.00065}_{-0.00062}$	$0.02245^{+0.00046}_{-0.00047}$	$0.02182^{+0.00082}_{-0.00077}$
$\Omega_c h^2$	$0.1229^{+0.0049}_{-0.0047}$	$0.1267^{+0.0062}_{-0.0061}$	$0.1234^{+0.0045}_{-0.0043}$	$0.1262^{+0.0058}_{-0.0056}$	$0.1219^{+0.0027}_{-0.0028}$	0.1222 ± 0.0032	$0.1222^{+0.0043}_{-0.0044}$	$0.1253^{+0.0058}_{-0.0059}$
100θ	$1.04045^{+0.00096}_{-0.00097}$	1.0399 ± 0.0011	$1.04045^{+0.00094}_{-0.00097}$	$1.0401^{+0.0010}_{-0.0011}$	$1.04065^{+0.00081}_{-0.00080}$	$1.04060^{+0.00084}_{-0.00085}$	$1.04059^{+0.00091}_{-0.00092}$	1.0401 ± 0.0010
τ	$0.088^{+0.039}_{-0.038}$	$0.074^{+0.047}_{-0.043}$	$0.084^{+0.040}_{-0.039}$	$0.076^{+0.049}_{-0.043}$	0.090 ± 0.038	$0.091^{+0.046}_{-0.043}$	0.078 ± 0.034	$0.062^{+0.038}_{-0.037}$
m_a(eV)	< 1.97	nb	< 1.09	< 1.63	< 0.929	< 1.07	< 1.45	< 2.15
n_S	$0.974^{+0.014}_{-0.015}$	…	0.974 ± 0.012	…	0.978 ± 0.010	…	$0.977^{+0.012}_{-0.013}$	…
$\ln[10^{10} A_s]$	$3.119^{+0.075}_{-0.074}$	…	3.112 ± 0.077	…	$3.121^{+0.076}_{-0.075}$	…	$3.096^{+0.062}_{-0.061}$	…
H_0(Km s^{-1} Mpc^{-1})	$67.9^{+2.4}_{-2.8}$	65.2 ± 3.4	$68.1^{+2.0}_{-2.3}$	$66.3^{+2.9}_{-3.1}$	68.8 ± 1.1	68.4 ± 1.3	$68.4^{+2.2}_{-2.5}$	66.0 ± 3.0
σ_8	$0.799^{+0.063}_{-0.086}$	$0.800^{+0.099}_{-0.097}$	$0.812^{+0.045}_{-0.050}$	$0.801^{+0.066}_{-0.070}$	$0.817^{+0.044}_{-0.049}$	$0.859^{+0.078}_{-0.081}$	$0.794^{+0.046}_{-0.059}$	$0.804^{+0.076}_{-0.085}$
$P_{s,1}$	$\equiv 1.307$	< 7.36	$\equiv 1.297$	< 8.0	$\equiv 1.262$	< 7.93	$\equiv 1.242$	< 7.95
$P_{s,2}$	$\equiv 1.138$	$1.18^{+0.40}_{-0.37}$	$\equiv 1.131$	$1.16^{+0.41}_{-0.37}$	$\equiv 1.123$	$1.12^{+0.39}_{-0.36}$	$\equiv 1.100$	$1.18^{+0.40}_{-0.37}$
$P_{s,3}$	$\equiv 1.119$	$0.71^{+0.39}_{-0.37}$	$\equiv 1.112$	$0.72^{+0.41}_{-0.40}$	$\equiv 1.107$	$0.76^{+0.41}_{-0.39}$	$\equiv 1.083$	0.68 ± 0.37
$P_{s,4}$	$\equiv 1.101$	1.20 ± 0.27	$\equiv 1.093$	$1.20^{+0.27}_{-0.26}$	$\equiv 1.091$	$1.22^{+0.27}_{-0.26}$	$\equiv 1.067$	1.19 ± 0.26
$P_{s,5}$	$\equiv 1.082$	1.09 ± 0.12	$\equiv 1.075$	$1.08^{+0.12}_{-0.11}$	$\equiv 1.076$	$1.08^{+0.13}_{-0.12}$	$\equiv 1.051$	$1.057^{+0.099}_{-0.098}$
$P_{s,6}$	$\equiv 1.064$	$1.070^{+0.093}_{-0.089}$	$\equiv 1.057$	$1.071^{+0.093}_{-0.083}$	$\equiv 1.061$	$1.072^{+0.097}_{-0.095}$	$\equiv 1.036$	$1.043^{+0.064}_{-0.066}$
$P_{s,7}$	$\equiv 1.046$	$1.047^{+0.090}_{-0.081}$	$\equiv 1.039$	$1.042^{+0.091}_{-0.086}$	$\equiv 1.045$	$1.056^{+0.095}_{-0.087}$	$\equiv 1.020$	$1.011^{+0.064}_{-0.059}$
$P_{s,8}$	$\equiv 1.029$	$1.003^{+0.093}_{-0.089}$	$\equiv 1.021$	$1.007^{+0.097}_{-0.091}$	$\equiv 1.031$	$1.028^{+0.097}_{-0.093}$	$\equiv 1.005$	$0.974^{+0.072}_{-0.066}$
$P_{s,9}$	$\equiv 1.011$	$0.988^{+0.092}_{-0.087}$	$\equiv 1.004$	$0.991^{+0.097}_{-0.090}$	$\equiv 1.016$	$1.021^{+0.095}_{-0.091}$	$\equiv 0.990$	$0.964^{+0.073}_{-0.072}$
$P_{s,10}$	$\equiv 0.994$	$1.00^{+0.10}_{-0.09}$	$\equiv 0.987$	$0.987^{+0.099}_{-0.095}$	$\equiv 1.001$	$1.03^{+0.11}_{-0.10}$	$\equiv 0.975$	$0.986^{+0.084}_{-0.082}$
$P_{s,11}$	$\equiv 0.978$	< 3.69	$\equiv 0.971$	$0.90^{+0.75}_{-0.56}$	$\equiv 0.987$	$2.6^{+1.9}_{-2.5}$	$\equiv 0.961$	$2.5^{+1.5}_{-1.7}$
$P_{s,12}$	$\equiv 0.896$	nb	$\equiv 0.890$	< 3.41	$\equiv 0.917$	nb	$\equiv 0.890$	nb

TABLE XI. Thermal axion: as Table III, but for the $\Lambda\mathrm{CDM} + m_a$ model.

Parameter	Planck TT, TE, EE + lowP		Planck TT, TE, EE + lowP + MPkW		Planck TT, TE, EE + lowP + BAO		Planck TT, TE, EE + lowP + lensing	
$\Omega_b h^2$	0.02248 ± 0.00032	$0.02241^{+0.00039}_{-0.00038}$	$0.02245^{+0.00030}_{-0.00031}$	$0.02236^{+0.00037}_{-0.00038}$	$0.02250^{+0.00030}_{-0.00029}$	$0.02248^{+0.00038}_{-0.00036}$	$0.02248^{+0.00033}_{-0.00030}$	$0.02242^{+0.00039}_{-0.00038}$
$\Omega_c h^2$	$0.1232^{+0.0034}_{-0.0036}$	$0.1233^{+0.0041}_{-0.0043}$	$0.1236^{+0.0032}_{-0.0033}$	$0.1241^{+0.0037}_{-0.0040}$	$0.1224^{+0.0023}_{-0.0024}$	0.1223 ± 0.0029	$0.1231^{+0.0032}_{-0.0033}$	$0.1224^{+0.0039}_{-0.0043}$
100θ	$1.04030^{+0.00065}_{-0.00067}$	$1.04020^{+0.00066}_{-0.00064}$	1.04029 ± 0.00065	$1.04022^{+0.00068}_{-0.00067}$	$1.04047^{+0.00059}_{-0.00060}$	$1.04045^{+0.00059}_{-0.00057}$	1.04037 ± 0.00066	1.04027 ± 0.00063
τ	$0.090^{+0.033}_{-0.034}$	$0.090^{+0.043}_{-0.042}$	0.087 ± 0.034	0.091 ± 0.039	0.092 ± 0.034	$0.093^{+0.043}_{-0.042}$	0.075 ± 0.028	$0.071^{+0.034}_{-0.032}$
m_a(eV)	< 2.09	< 2.44	< 1.19	< 1.90	< 0.741	< 1.19	< 1.68	< 2.44
n_S	$0.972^{+0.011}_{-0.012}$	⋯	0.9734 ± 0.0098	⋯	$0.9754^{+0.0092}_{-0.0089}$	⋯	$0.974^{+0.010}_{-0.011}$	⋯
$\ln[10^{10} A_s]$	$3.125^{+0.065}_{-0.067}$	⋯	$3.119^{+0.067}_{-0.068}$	⋯	3.125 ± 0.067	⋯	3.092 ± 0.053	⋯
H_0(Km s^{-1} Mpc^{-1})	$67.6^{+1.9}_{-2.2}$	66.8 ± 2.2	$67.9^{+1.6}_{-1.8}$	$67.3^{+2.0}_{-2.1}$	68.6 ± 1.0	68.5 ± 1.1	$67.9^{+1.9}_{-2.0}$	$66.9^{+2.1}_{-1.9}$
σ_8	$0.798^{+0.067}_{-0.090}$	$0.806^{+0.11}_{-0.10}$	$0.815^{+0.045}_{-0.054}$	$0.801^{+0.068}_{-0.078}$	$0.827^{+0.037}_{-0.039}$	$0.871^{+0.072}_{-0.084}$	$0.788^{+0.051}_{-0.066}$	$0.790^{+0.092}_{-0.085}$
$P_{s,1}$	$\equiv 1.339$	< 7.74	$\equiv 1.319$	< 7.85	$\equiv 1.302$	< 7.71	$\equiv 1.272$	< 7.74
$P_{s,2}$	$\equiv 1.154$	$1.15^{+0.39}_{-0.36}$	$\equiv 1.143$	$1.14^{+0.40}_{-0.36}$	$\equiv 1.141$	$1.12^{+0.39}_{-0.36}$	$\equiv 1.108$	$1.18^{+0.40}_{-0.37}$
$P_{s,3}$	$\equiv 1.133$	$0.72^{+0.40}_{-0.37}$	$\equiv 1.123$	$0.74^{+0.38}_{-0.37}$	$\equiv 1.122$	$0.74^{+0.40}_{-0.38}$	$\equiv 1.090$	$0.68^{+0.37}_{-0.34}$
$P_{s,4}$	$\equiv 1.113$	1.25 ± 0.24	$\equiv 1.103$	1.24 ± 0.23	$\equiv 1.104$	1.24 ± 0.23	$\equiv 1.071$	$1.23^{+0.23}_{-0.22}$
$P_{s,5}$	$\equiv 1.093$	$1.11^{+0.12}_{-0.11}$	$\equiv 1.084$	$1.11^{+0.11}_{-0.10}$	$\equiv 1.086$	$1.10^{+0.12}_{-0.11}$	$\equiv 1.053$	$1.071^{+0.092}_{-0.088}$
$P_{s,6}$	$\equiv 1.073$	$1.089^{+0.098}_{-0.091}$	$\equiv 1.065$	$1.087^{+0.083}_{-0.081}$	$\equiv 1.069$	$1.077^{+0.096}_{-0.088}$	$\equiv 1.036$	$1.013^{+0.064}_{-0.059}$
$P_{s,7}$	$\equiv 1.054$	$1.058^{+0.090}_{-0.087}$	$\equiv 1.047$	$1.061^{+0.079}_{-0.077}$	$\equiv 1.052$	$1.056^{+0.094}_{-0.087}$	$\equiv 1.018$	$1.013^{+0.064}_{-0.059}$
$P_{s,8}$	$\equiv 1.035$	$1.035^{+0.091}_{-0.085}$	$\equiv 1.029$	$1.037^{+0.080}_{-0.079}$	$\equiv 1.035$	$1.036^{+0.093}_{-0.085}$	$\equiv 1.001$	$0.995^{+0.066}_{-0.060}$
$P_{s,9}$	$\equiv 1.016$	$1.020^{+0.088}_{-0.083}$	$\equiv 1.011$	$1.020^{+0.080}_{-0.078}$	$\equiv 1.018$	$1.027^{+0.090}_{-0.089}$	$\equiv 0.984$	$0.982^{+0.067}_{-0.061}$
$P_{s,10}$	$\equiv 0.998$	$1.03^{+0.10}_{-0.09}$	$\equiv 0.993$	$1.009^{+0.088}_{-0.085}$	$\equiv 1.002$	1.04 ± 0.10	$\equiv 0.968$	$0.998^{+0.079}_{-0.071}$
$P_{s,11}$	$\equiv 0.980$	$2.8^{+1.6}_{-2.4}$	$\equiv 0.976$	$0.94^{+1.0}_{-0.8}$	$\equiv 0.985$	$2.9^{+1.8}_{-2.6}$	$\equiv 0.952$	$3.1^{+1.4}_{-1.7}$
$P_{s,12}$	$\equiv 0.892$	< 8.89	$\equiv 0.891$	< 3.06	$\equiv 0.906$	< 8.66	$\equiv 0.872$	nb

[1] A. H. Guth, Phys. Rev. D **23**, 347 (1981).
[2] A. D. Linde, Phys. Lett. **108B**, 389 (1982).
[3] A. A. Starobinsky, Phys. Lett. **117B**, 175 (1982).
[4] S. W. Hawking, Phys. Lett. **115B**, 295 (1982).
[5] A. Albrecht and P. J. Steinhardt, Phys. Rev. Lett. **48**, 1220 (1982).
[6] V. F. Mukhanov, H. A. Feldman, and R. H. Brandenberger, Phys. Rep. **215**, 203 (1992).
[7] V. F. Mukhanov and G. V. Chibisov, Pis'ma Zh. Eksp. Teor. Fiz. **33**, 549 (1981) [JETP Lett. **33**, 532 (1981)].
[8] F. Lucchin and S. Matarrese, Phys. Rev. D **32**, 1316 (1985).
[9] D. H. Lyth and A. Riotto, Phys. Rep. **314**, 1 (1999).
[10] B. A. Bassett, S. Tsujikawa, and D. Wands, Rev. Mod. Phys. **78**, 537 (2006).
[11] D. Baumann and H. V. Peiris, Adv. Sci. Lett. **2**, 105 (2009).
[12] A. E. Romano and A. G. Cadavid, Eur. Phys. J. C **75**, 589 (2015).
[13] N. Kitazawa and A. Sagnotti, J. Cosmol. Astropart. Phys. 04 (2014) 017.
[14] J. Martin, C. Ringeval, and V. Vennin, Phys. Dark Univ. **5–6**, 75 (2014).
[15] J. Chluba, J. Hamann, and S. P. Patil, Int. J. Mod. Phys. D **24**, 1530023 (2015).
[16] A. Shafieloo and T. Souradeep, Phys. Rev. D **70**, 043523 (2004).
[17] G. Nicholson and C. R. Contaldi, J. Cosmol. Astropart. Phys. 07 (2009) 011.
[18] D. K. Hazra, A. Shafieloo, and T. Souradeep, Phys. Rev. D **87**, 123528 (2013).
[19] D. K. Hazra, A. Shafieloo, and T. Souradeep, J. Cosmol. Astropart. Phys. 11 (2014) 011.
[20] G. Nicholson, C. R. Contaldi, and P. Paykari, J. Cosmol. Astropart. Phys. 01 (2010) 016.
[21] P. Hunt and S. Sarkar, J. Cosmol. Astropart. Phys. 01 (2014) 025.
[22] P. Hunt and S. Sarkar, J. Cosmol. Astropart. Phys. 12 (2015) 052.
[23] G. Goswami and J. Prasad, Phys. Rev. D **88**, 023522 (2013).
[24] M. Matsumiya, M. Sasaki, and J. Yokoyama, Phys. Rev. D **65**, 083007 (2002).
[25] M. Matsumiya, M. Sasaki, and J. Yokoyama, J. Cosmol. Astropart. Phys. 02 (2003) 003.
[26] N. Kogo, M. Matsumiya, M. Sasaki, and J. Yokoyama, Astrophys. J. **607**, 32 (2004).
[27] N. Kogo, M. Sasaki, and J. Yokoyama, Prog. Theor. Phys. **114**, 555 (2005).
[28] R. Nagata and J. Yokoyama, Phys. Rev. D **78**, 123002 (2008).
[29] P. A. R. Ade *et al.* (Planck Collaboration), arXiv:1502.02114.
[30] C. L. Bennett *et al.* (WMAP Collaboration), Astrophys. J. Suppl. Ser. **208**, 20 (2013).
[31] P. A. R. Ade *et al.*, Astron. Astrophys. **571**, A1 (2014).
[32] R. Adam *et al.*, arXiv:1502.01582.
[33] R. de Putter, E. V. Linder, and A. Mishra, Phys. Rev. D **89**, 103502 (2014).
[34] S. Gariazzo, C. Giunti, and M. Laveder, J. Cosmol. Astropart. Phys. 04 (2015) 023.
[35] E. Di Valentino, S. Gariazzo, E. Giusarma, and O. Mena, Phys. Rev. D **91**, 123505 (2015).
[36] S. Gariazzo, L. Lopez-Honorez, and O. Mena, Phys. Rev. D **92**, 063510 (2015).
[37] A. Lewis, A. Challinor, and A. Lasenby, Astrophys. J. **538**, 473 (2000).
[38] A. Lewis and S. Bridle, Phys. Rev. D **66**, 103511 (2002).
[39] P. A. R. Ade *et al.*, arXiv:1502.01589.
[40] G. Mangano, G. Miele, S. Pastor, T. Pinto, O. Pisanti, and P. D. Serpico, Nucl. Phys. **B729**, 221 (2005).
[41] F. Fritsch and R. Carlson, SIAM J. Numer. Anal. **17**, 238 (1980).
[42] F. Fritsch and J. Butland, SIAM J. Sci. Stat. Comput. **5**, 300 (1984).
[43] N. Aghanim *et al.*, arXiv:1507.02704.
[44] F. Beutler, C. Blake, M. Colless, D. H. Jones, L. Staveley-Smith, L. Campbell, Q. Parker, W. Saunders, and F. Watson, Mon. Not. R. Astron. Soc. **416**, 3017 (2011).
[45] A. J. Ross, L. Samushia, C. Howlett, W. J. Percival, A. Burden, and M. Manera, Mon. Not. R. Astron. Soc. **449**, 835 (2015).
[46] L. Anderson *et al.* (BOSS Collaboration), Mon. Not. R. Astron. Soc. **441**, 24 (2014).
[47] D. Parkinson *et al.*, Phys. Rev. D **86**, 103518 (2012).
[48] P. A. R. Ade *et al.*, arXiv:1502.01591.
[49] Z. Hou, R. Keisler, L. Knox, M. Millea, and C. Reichardt, Phys. Rev. D **87**, 083008 (2013).
[50] J. Lesgourgues, G. Mangano, G. Miele, and S. Pastor, *Neutrino Cosmology* (Cambridge University Press, Cambridge, England, 2013).
[51] M. Archidiacono, E. Giusarma, S. Hannestad, and O. Mena, Adv. High Energy Phys. **2013**, 191047 (2013).
[52] S. Gariazzo, C. Giunti, M. Laveder, Y. F. Li, and E. M. Zavanin, J. Phys. G **43**, 033001 (2016).
[53] B. A. Reid, L. Verde, R. Jimenez, and O. Mena, J. Cosmol. Astropart. Phys. 01 (2010) 003.
[54] J. Hamann, S. Hannestad, J. Lesgourgues, C. Rampf, and Y. Y. Y. Wong, J. Cosmol. Astropart. Phys. 07 (2010) 022.
[55] R. de Putter *et al.*, Astrophys. J. **761**, 12 (2012).
[56] E. Giusarma, R. De Putter, and O. Mena, Phys. Rev. D **87**, 043515 (2013).
[57] G.-B. Zhao *et al.*, Mon. Not. R. Astron. Soc. **436**, 2038 (2013).
[58] Z. Hou *et al.*, Astrophys. J. **782**, 74 (2014).
[59] M. Archidiacono, E. Giusarma, A. Melchiorri, and O. Mena, Phys. Rev. D **87**, 103519 (2013).
[60] E. Giusarma, R. de Putter, S. Ho, and O. Mena, Phys. Rev. D **88**, 063515 (2013).
[61] S. Riemer-Srensen, D. Parkinson, and T. M. Davis, Phys. Rev. D **89**, 103505 (2014).
[62] J.-W. Hu, R.-G. Cai, Z.-K. Guo, and B. Hu, J. Cosmol. Astropart. Phys. 05 (2014) 020.
[63] E. Giusarma, E. Di Valentino, M. Lattanzi, A. Melchiorri, and O. Mena, Phys. Rev. D **90**, 043507 (2014).
[64] E. Di Valentino, E. Giusarma, O. Mena, A. Melchiorri, and J. Silk, arXiv:1511.00975.
[65] P. A. R. Ade *et al.*, Astron. Astrophys. **571**, A16 (2014).
[66] K. N. Abazajian *et al.*, arXiv:1204.5379.
[67] J. Kopp, P. A. N. Machado, M. Maltoni, and T. Schwetz, J. High Energy Phys. 05 (2013) 050.
[68] M. C. Gonzalez-Garcia, M. Maltoni, and T. Schwetz, arXiv:1512.06856.

[69] R. D. Peccei and H. R. Quinn, Phys. Rev. Lett. **38**, 1440 (1977).
[70] R. D. Peccei and H. R. Quinn, Phys. Rev. D **16**, 1791 (1977).
[71] S. Weinberg, Phys. Rev. Lett. **40**, 223 (1978).
[72] F. Wilczek, Phys. Rev. Lett. **40**, 279 (1978).
[73] K. A. Olive *et al.* (Particle Data Group), Chin. Phys. C **38**, 090001 (2014).
[74] M. Archidiacono, T. Basse, J. Hamann, S. Hannestad, G. Raffelt, and Y. Y. Y. Wong, J. Cosmol. Astropart. Phys. 05 (2015) 050.
[75] A. Melchiorri, O. Mena, and A. Slosar, Phys. Rev. D **76**, 041303 (2007).
[76] S. Hannestad, A. Mirizzi, G. G. Raffelt, and Y. Y. Y. Wong, J. Cosmol. Astropart. Phys. 08 (2007) 015.
[77] S. Hannestad, A. Mirizzi, G. G. Raffelt, and Y. Y. Y. Wong, J. Cosmol. Astropart. Phys. 04 (2008) 019.
[78] S. Hannestad, A. Mirizzi, G. G. Raffelt, and Y. Y. Y. Wong, J. Cosmol. Astropart. Phys. 08 (2010) 001.
[79] M. Archidiacono, S. Hannestad, A. Mirizzi, G. Raffelt, and Y. Y. Y. Wong, J. Cosmol. Astropart. Phys. 10 (2013) 020.
[80] E. Di Valentino, E. Giusarma, M. Lattanzi, O. Mena, A. Melchiorri, and J. Silk, Phys. Lett. B **752**, 182 (2016).
[81] E. Di Valentino, A. Melchiorri, and J. Silk, Phys. Rev. D **92**, 121302 (2015).